Title
Observations of ozone and related species in the northeast Pacific during the PHOBEA campaigns 2. Airborne observations

Journal
Journal of Geophysical Research Atmospheres, 106(D7)

ISSN
0148-0227

Authors
Kotchenruther, RA
Jaffe, DA
Beine, HJ
et al.

Publication Date
2001-04-16

DOI
10.1029/2000JD900425

JOURNAL OF GEOPHYSICAL RESEARCH, VOL. 106, NO. D7, PAGES 7463-7483, APRIL 16, 2001

Observations of ozone and related species in the northeast Pacific during the PHOBEA campaigns 2. Airborne observations

Robert A. Kotchenruther,[1] Daniel A. Jaffe,[2] Harald J. Beine,[3]
Theodore L. Anderson,[4] Jan W. Bottenheim,[5] Joyce M. Harris,[6]
Donald R. Blake,[7] and Rainer Schmitt[8]

Abstract. During late March and April of 1999 the University of Wyoming's King Air research aircraft measured atmospheric concentrations of NO, O_3, peroxyacetyl nitrate (PAN), CO, CH_4, VOCs, aerosols, and $J(NO_2)$ off the west coast of the United States. During 14 flights, measurements were made between 39°-48°N latitude, 125°-129°W longitude, and at altitudes from 0-8 km. These flights were part of the Photochemical Ozone Budget of the Eastern North Pacific Atmosphere (PHOBEA) experiment, which included both ground-based and airborne measurements. Flights were scheduled when meteorological conditions minimized the impact of local pollution sources. The resulting measurements were segregated by air mass source region as indicated by back isentropic trajectory analysis. The chemical composition of marine air masses whose 5-day back isentropic trajectories originated north of 40°N latitude or west of 180°W longitude (WNW) differed significantly from marine air masses whose 5-day back isentropic trajectories originated south of 40°N latitude and east of 180°W longitude (SW). Trajectory and chemical analyses indicated that the majority of all encountered air masses, both WNW and SW, likely originated from the northwestern Pacific and have characteristics of emissions from the East Asian continental region. However, air masses with WNW back trajectories contained higher mixing ratios of NO, NO_x, O_3, PAN, CO, CH_4, various VOC pollution tracers, and aerosol number concentration, compared to those air masses with SW back trajectories. Calculations of air mass age using two separate methods, photochemical and back trajectory, are consistent with transport from the northwestern Pacific in 8-10 days for air masses with WNW back trajectories and 16-20 days for air masses with SW back trajectories. Correlations, trajectory analysis, and comparisons with measurements made in the northwestern Pacific during NASA's Pacific Exploritory Mission-West Phase B (PEM-West B) experiment in 1994 are used to investigate the data. These analyses provide evidence that anthropogenically influenced air masses from the northwestern Pacific affect the overall chemical composition of the northeastern Pacific troposphere.

1. Introduction

The East Asian region is a large and growing source of anthropogenic emissions [*Akimoto and Narita*, 1994; *Elliott et al.*, 1997; *VanAardeen et al.*, 1999]. For example, from 1975 to 1987, emissions of both NO_x and SO_2 from the East Asian region increased at an average rate of 4% per year [*Akimoto and Narita*, 1994]. It is well established that these and other anthropogenic pollutants are transported from East Asia into the central North Pacific [*Ridley et al.*, 1997; *Gregory et al.*, 1997; *Talbot et al.*, 1997]. During aircraft measurements off the coast of Washington State in the spring of 1985, *Andreae et al.* [1988] attributed enhancements of SO_2 and non-sea-salt SO_4^{2-} in the free troposphere to long-range transport from Asia within 4-8 days. Measurements of light hydrocarbons and other trace gases were also made at Point Arena California in the spring of 1985 [*Parrish et al.*, 1992]. In that study, Parrish et al. attributed variations in the ratios of selected hydrocarbons to different degrees of photochemical aging from a continental source, which was assumed to be Asian. Measurements made during the spring of 1997 at Cheeka Peak Observatory (CPO), a ground-based site on the coast of Washington State, also showed that anthropogenic trace gases from the Asian continent can reach the coast of Washington State during rapid transport events [*Jaffe et al.*, 1999]. Several studies in Canada on persistent organochlorine compounds have attributed elevated concentrations, in both air and water,

[1]Department of Chemistry, University of Washington, Seattle, Washington.
[2]Interdisciplinary Arts and Sciences, University of Washington, Bothell, Washington.
[3]CNR-Istituto sull'Inquinamento Atmosferico, Rome, Italy.
[4]Department of Atmospheric Sciences, University of Washington, Seattle, Washington.
[5]Atmospheric Environment Service, Toronto, Ontario, Canada.
[6]Climate Monitoring and Diagnostics Laboratory, NOAA, Boulder, Colorado.
[7]Department of Chemistry, University of California, Irvine, California.
[8]Meteorologie Consult GmbH, Glashütten, Germany.

Paper number 2000JD900425.
0148-0227/01/2000JD900425$09.00

to long-range transport from Asia [*Blais et al.*, 1998; *Bailey et al.*, 2000].

In addition to the individual transport events described above, Asian emissions likely impact the background chemical composition of the North Pacific atmosphere. *Berntsen et al.* [1999] recently employed a global three-dimentional chemical transport model to determine the impact of Asian industrial emissions on air arriving to North America. Their model calculations estimated that 10, 20, and 30% of the O_3, CO, and peroxyacetyl nitrate (PAN), respectively, in air arriving to North America during spring resulted from Asian industrial emissions.

The winter and springtime North Pacific atmosphere is characterized by strong zonal flow from the Asian continent and strong midlatitude westerly winds across the Pacific Ocean. The eastern North Pacific during springtime is characterized by a region of low sea level pressure usually centered east of the Aleutian Islands (often called the "Aleutian low") and a broader region of high sea level pressure situated northeast of the Hawaiian Islands. The combined cyclonic and anticyclonic rotation of the Aleutian low and northeastern Pacific high, respectively, direct the strongest midlatitude westerly flow into the northwestern United States.

Near 180°W longitude the climatological midlatitude "Japan" jet stream splits into a weaker subtropical jet centered above 15° to 20°N latitude and a continuing midlatitude jet centered above 40° to 45°N latitude. The usual placement of the midlatitude jet directs frequent winter and springtime frontal systems, generated from short wave disturbances in the Aleutian low, into northwestern Canada and the United States. These frontal systems are often associated with tropopause folds, which transport ozone-rich stratospheric air into the troposphere.

In the spring of 1994, aircraft measurements of trace gases were made over the northwestern Pacific ocean as part of the Pacific Exploratory Mission-West Phase B (PEM-West B) [*Hoell et al.*, 1997]. The PEM-West B experiment made measurements in the Asian continental outflow during springtime. In this paper we present a similar set of trace gas measurements made during the spring of 1999 over the northeastern Pacific Ocean and compare our measurements to those made during PEM-West B.

Other aircraft measurements of trace gases in the North Pacific include (1) NASA's Global Tropospheric Experiment/Chemical Instrumentation Test and Evaluation programs 1 [*Ridley et al.*, 1989] and 2 [*Hübler et al.*, 1992] conducted in 1983/1984 and 1986, respectively, (2) PEM-West Phase A, conducted in the northwestern Pacific during the summer of 1991 [*Hoell et al.*, 1996], and (3) aircraft measurements made as part of the second Mauna Loa Observatory Photochemistry Experiment in the spring of 1992 [*Ridley et al.*, 1997].

The measurements described in this paper were part of the Photochemical Ozone Budget of the Eastern North Pacific Atmosphere (PHOBEA) experiment, which included both ground-based measurements at CPO [*Jaffe et al.*, this issue] and airborne measurements. The primary goals of the PHOBEA experiment were to quantify the ozone photochemical tendency over the remote northeastern Pacific Ocean, investigate the impact of springtime PAN decomposition on the ozone photochemical tendency, and investigate the impacts of long-range transport of Asian anthropogenic emissions on the chemical composition of air over the northeastern Pacific Ocean. This work presents the measurements made with the King Air and explores long-range transport issues. Future publications will investigate the ozone photochemical tendency and the impacts of PAN thermal decomposition over the northeastern Pacific Ocean.

2. Experiment

From March 26 to April 28, 1999, the University of Wyoming's Beech Super King Air 200T aircraft made 14 flights over the northeastern Pacific Ocean between 39°-48°N latitude, 125°-129°W longitude, and at altitudes between 0-8 km. The King Air was equipped with instrumentation to measure NO, O_3, peroxyacetyl nitrate (PAN), CO, CH_4, volatile organic compounds (VOCs), aerosols (particle count, light scattering, and light absorption), and $J(NO_2)$. The aircraft was also outfitted with standard meteorological instrumentation and was pressurized. Raw data were recorded as 1-s averages into the aircraft's data system, except for PAN and NO, which stored data in separate data loggers. Pressurized whole air samples were collected in stainless steel canisters and analyzed later for CO, CH_4, and VOCs. A detailed description of the instrumentation used to make these measurements can be found in Appendix A at the end of this paper.

All flights originated and ended at Paine Field in Everett, Washington (47.9°N and 122.3°W), which is located approximately 30 miles north of Seattle. Instrumentation on board the King Air was turned on as much as 3 hours before takeoff, depending on the warm-up time required. To avoid contaminating the instruments during warm-up, aircraft taxi, and takeoff, instruments were flushed with either "zero air" from pressurized cylinders or with charcoal scrubbed ambient air. Instruments were switched from these relatively clean sources to ambient air approximately 5 to 10 min after takeoff. All instrumentation was turned off prior to landing.

Research flights were divided into a number of flight "legs." A typical flight consisted of a 1000 (local time) take-

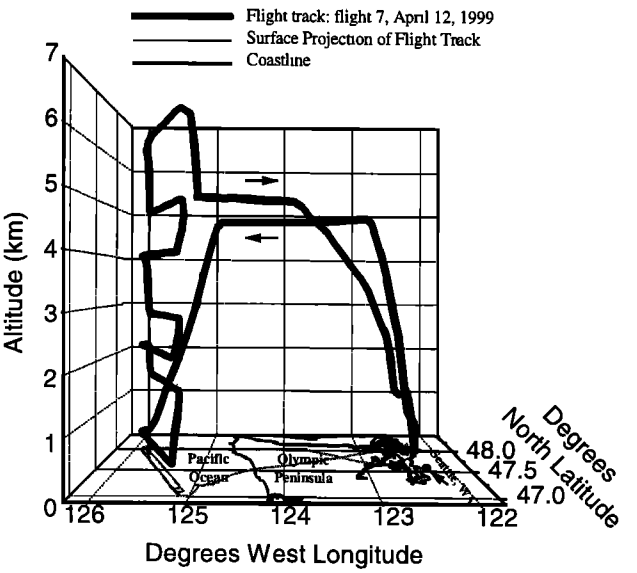

Figure 1. Typical flight track of the King Air during the PHOBEA experiment.

off and approximately 30 min in an outbound ferry leg to the sampling region off the coast of Washington State. Flights were scheduled to maximize the amount of time spent in the experiment area during high Sun conditions. Local noon was at approximately 1230 LT. The outbound ferry leg was used primarily for instrument calibration and to confirm that all instruments were functioning normally. Sampling during each flight was done over the Pacific Ocean in 6 to 10 level flight legs of 20 min duration. There were roughly 5 min between each leg, which were used to change heading and altitude in order to set up for the next sampling leg. Figure 1 depicts a typical flight track. The only exception to this standard flight track was on April 21 (flight 11), where the King Air flew south down the coast of Oregon and into northern California making measurements at only two altitudes. This flight was used to investigate PAN decomposition in a strongly subsiding air mass off the coast of northern California. After measurements were completed in the sampling region, the inbound ferry leg back to Paine Field was used for further instrument calibrations and to shut down the instruments prior to landing.

Operational forecasting for King Air flights was conducted with the goal of sampling air off the coast of Washington State that had not recently (within 3 days) been exposed to continental influence. Primarily, this meant forecasting for westerly, southwesterly, or northwesterly winds throughout the lower troposphere in the region where sampling would take place. Additionally, flights were not scheduled when frontal systems were present. We avoided fronts in part to minimize the impact of stratospheric air on our measurements, which can occur during tropopause folds, but also to avoid air parcels in which rapid and unpredictable changes in vertical and horizontal motion occurred. Such unpredictability makes the determination of source regions through back trajectories more difficult Several numerical models, run in forecast mode, were consulted and compared before conducting flights. Additionally, gridded data from atmospheric forecast models were used to generate forecasted back trajectories, and 24 to 72 hour forecasted back trajectories were used to estimate the likelihood that air parcels in the experiment area had avoided recent exposure to the North American continent.

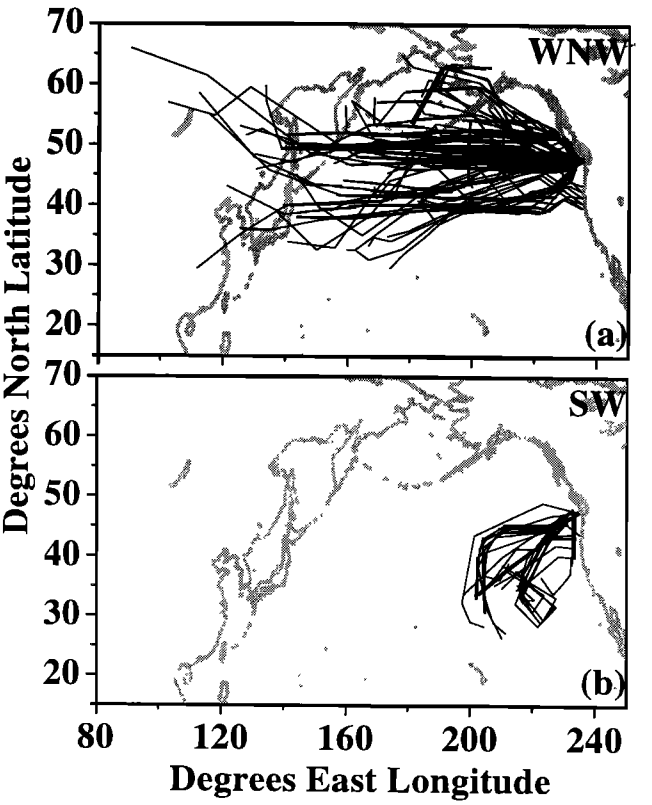

Figure 2. Five-day back isentropic trajectories for the PHOBEA aircraft experiment and segregated into two regimes; (a) west and northwest (WNW), where the back trajectory origin is north of 40°N latitude or west of 180°W longitude, and (b) southwest (SW), where the back trajectory origin is south of 40°N latitude and east of 180°W longitude.

3. Data Analysis and Discussion

3.1. Air Mass Trajectory Analysis

Back isentropic trajectories were calculated to determine the source regions for air masses encountered during aircraft sampling. Forward isentropic trajectories were used to estimate the impacts of air, originating over Asia, on various regions across the Pacific Ocean. Trajectories were obtained from two sources: the National Oceanic and Atmospheric Administration's (NOAA) Climate Monitoring and Diagnostics Laboratory (CMDL) using the European Centre for Medium Range Weather Forecasts (ECMWF) gridded data set and NOAA's Air Resources Laboratory (ARL) using the Hybrid Single-Particle Lagrangian Integrated Trajectory (HYSPLIT4) model, 1997 (http://www.arl.noaa.gov/ready/hysplit4.html) with the National Center for Environmental Prediction's (NCEP) "final model run" (FNL) meteorological data set. Trajectories of 10 day duration were available from NOAA CMDL starting every 12 hours, and those of 5 day duration were available from NOAA ARL starting every hour. We used NOAA CMDL as our primary source of trajectory data (exceptions are discussed below). There was generally good agreement between the CMDL and ARL trajectories. Because of the different time duration of NOAA CMDL and NOAA ARL trajectories, 10 and 5 days, respectively, we use only 5 day trajectories from both data sets for consistency.

Aircraft data were separated into three categories based on source region as determined from 5-day back isentropic trajectories. The categories were (1) continental North America: those that crossed over the North American continent within 3 days, (2) westerly and northwesterly (WNW): those trajectories originating 5 days upwind north of 40°N latitude or west of 180°W longitude, and (3) southwesterly (SW): those trajectories originating 5 days upwind south of 40°N and east of 180°W. Back trajectories were calculated for each 20 min flight leg using the mean latitude, longitude, and altitude as the starting point. Most flights were conducted between 1700 UT and 2200 UT. However, only 1200 UT and 0000 UT trajectory starting times were available from NOAA CMDL. Therefore both the 1200 UT and 0000 UT back trajectories bracketing the measurement were used to classify the air mass source region. In general, both showed the same source region. Rarely, when differing source regions were indicated, a back trajectory from NOAA ARL was used to "break the tie" and classify the source region. The resulting classifications resulted in a total of 1 continental North American back tra-

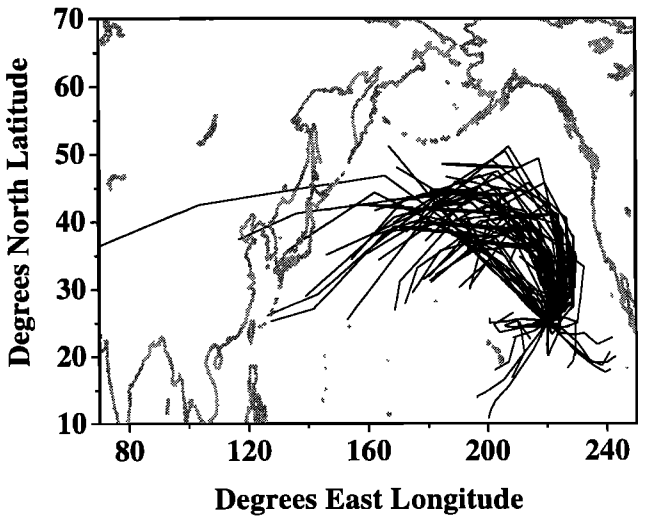

Figure 3. Five-day back isentropic trajectories starting at 25°N, 140°W, 5 km, at 12 hour intervals, and for the duration of the PHOBEA aircraft experiment.

jectory, 71 WNW, and 22 SW. Figure 2 shows a summary of all back trajectories for the WNW and SW regimes.

The frequency of trajectories arriving from the WNW and SW regimes was representative of the typical number of air masses arriving from each region for this time of year. A 4 year study of 5 day back isentropic trajectories arriving at CPO research station, from 1994-1997 and for the same time of year as the PHOBEA aircraft study, resulted in 65% of back trajectories originating from the WNW region, 29% from the SW region, and 6% from the North American continent.

It is reasonable to assume that the majority of air masses in the WNW regime originated from the northwestern Pacific without experiencing North American influence. However, because trade winds can advect air from North and Central America into the tropical and extratropical North Pacific, this may not be a reasonable assumption for air masses in the SW regime. In order to address this, back isentropic trajectories were calculated starting at 25°N, 140°W, at various altitudes, and over the period of the PHOBEA aircraft experiment. The location 25°N, 140°W represents the average 5 day origin in longitude and the most southerly origin in latitude of air masses with SW back trajectories. Figure 3 shows back trajectories, starting at 25°N, 140°W, 5 km, and for the duration of the PHOBEA aircraft experiment. While we present only trajectories arriving at 5 km, the vast majority of trajectories arriving at altitudes from 1-7 km had a westerly track indicating eastward transport from the northwestern Pacific.

We also calculated forward isentropic trajectories from four Asian cities, to determine their impact on the two regions of the eastern Pacific representing the source regions of the aircraft data. We chose four Asian cities spanning a range of latitudes from 20°-40°N; they are Hong Kong (22.18°N, 114.23°E), Shanghai (31.25°N, 121.43°E), Tokyo (35.75°N, 139.75°E), and Beijing (39.92°N, 116.33°E). Trajectories were started above these cities at an elevation of 3 km, at 12 hour increments, and for the duration of the PHOBEA aircraft experiment. We calculated the frequency of 5 day forward isentropic trajectories from each of these cities ending in two regions of the eastern Pacific. The two regions were defined by boxes (1) 180.0°W, 124.4°W, 60°N, and 40°N, which represents the source region for WNW back trajectories and (2) 180.0°W, 124.4°W, 40°N, and 25°N, which represents the source region for SW back trajectories. The percentage of 5 day forward trajectories ending in these regions is given in Table 1. These data indicate that the WNW region is generally twice as likely to be influenced by 5 day old air from these cities.

3.2. Data Quality Control to Remove Local Pollution Sources

Because the goals of the PHOBEA experiment are to investigate the chemistry and chemical composition of the remote troposphere, after completing the initial data processing and quality control for each instrument, the entire data set was further quality-controlled to exclude data where there was a reasonable possibility of contamination from local pollution sources. There were two sources of local pollution; exhaust plumes from local shipping and instances when continental air from North America passed over the experiment area.

Ship exhaust plumes were encountered in the boundary layer during flights 3, 5, and 6. These plumes were easily identified in the data record as large spikes in NO (of the order of 50 to 200 parts per trillion by volume (pptv) above the background) and elevated aerosol concentration. In each case of contamination a nearby ship was observed either visually or by aircraft radar. To remove the ship plume contamination from the data record, boundary layer data from flights 3, 5, and 6 were excluded from the analyses presented here unless NO was measured at the background level of 0-20 pptv and contaminated air had not been encountered for at least 2 min.

The influence of continental North American air, as a source of contamination of PHOBEA aircraft data, was determined from an analysis of back trajectories, NO, and aerosol data. This analysis indicated only one flight leg with evidence of continental North American influence. This occurred on April 16 (flight 9) in the boundary layer where the winds were southeasterly, NO mixing ratios averaged 110 pptv, aerosol concentrations were elevated, and the back tra-

Table 1. Percentage of 5 Day Forward Isentropic Trajectories Ending in the Latitude and Longitude Boxes Indicated[a]

Starting Latitude and Longitude (All Trajectories Started at an Altitude of 3 km)	Percent of 5 Day Forward Trajectories Ending Within 180 0°W, 124.4°W, 60°N, and 40°N for the Duration of the PHOBEA Experiment	Percent of 5 Day Forward Trajectories Ending Within 180.0°W, 124.4°W, 40°N, and 25°N for the Duration of the PHOBEA Experiment
22.18°N, 114.23°E (Hong Kong)	16.2	7 4
31.25°N, 121.43°E (Shanghai)	20.6	10.3
35.75°N, 139.75°E (Tokyo)	29 4	13.2
39.92°N, 116.33°E (Beijing)	20.6	8.8

[a]Trajectories were started at 3 km over the corresponding latitude and longitude of four Asian cities at 12 hour intervals and for the duration of the 1999 PHOBEA aircraft experiment.

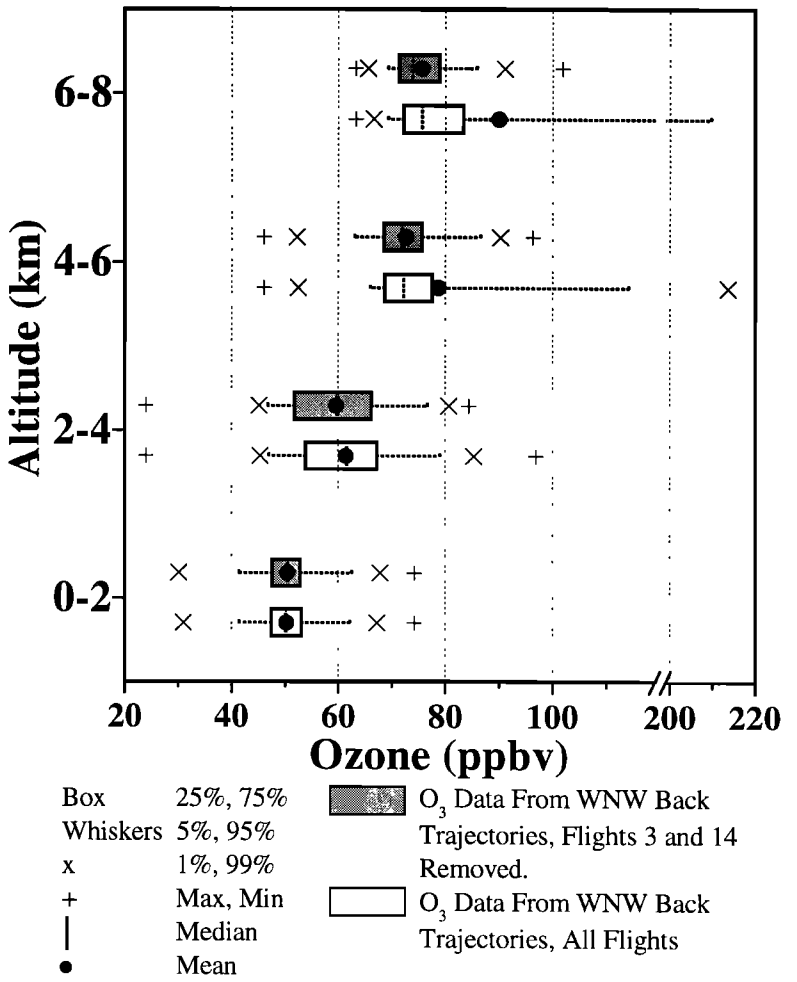

Figure 4. Box plots of ozone made from 1 min averages of the aircraft data. The effects of stratospheric air during flights 3 and 14 are indicated by plotting ozone data both including and excluding these flights.

jectory crossed over North America within 24 hours. Hence, in the subsequent analysis, boundary layer data from flight 9 were excluded. In all remaining flight legs, winds ranged from northwesterly to southerly and had back trajectories indicating eastward transport from the remote Pacific (see Figure 2). Air masses originating from the remote Pacific were typically either maritime polar with westerly or northwesterly back trajectories, or maritime tropical with southerly or southwesterly back trajectories.

3.3. Stratospheric Influence

There are two main sources of ozone in the troposphere; in situ production and transport from the stratosphere. A method of identifying intrusions of stratospheric air into the troposphere has been presented by *Cooper et al.* [1998]. They used enhanced satellite water vapor images to identify intrusions of dry air during postfrontal conditions and associated these dry air intrusions with high concentrations of ozone of stratospheric origin. They found that the ozone slope with height during postfrontal conditions was 6 to 12 ppbv km^{-1} in the lowest 8 km of the troposphere, whereas the prefrontal ozone slope averaged 2 ppbv km^{-1}.

In order to identify instances of direct stratospheric influence in the PHOBEA aircraft data, we performed a similar analysis. We found that during two flights, April 3 and 28 (flights 3 and 14), the ozone slope with height exceeded 6 ppbv km^{-1}; these two flights were also in the vicinity of significant dry air intrusions identified in satellite water vapor images. Ozone mixing ratios on these flights reached 311 ppbv and 132 ppbv, respectively, with very low mixing ratios of water vapor and other measured species.

All back trajectories from flights 3 and 14 fall in the WNW category. Figure 4 shows box plots of ozone mixing ratio with height, grouped in 2 km bins from 0 to 8 km. Box plots of WNW data, both including and excluding flights 3 and 14, are presented. The box plots indicate significant ozone enhancement from 4-8 km when data from flights 3 and 14 are included. However, there is no significant enhancement in ozone from 0-4 km when flights 3 and 14 are included. From this analysis we concluded that data from flights 3 and 14 between 4-8 km are significantly influenced by stratospheric air and excluded those data in the subsequent analyses where we compare WNW with SW air masses.

3.4. Data Averages

Each instrument on board the King Air aircraft, in general, made measurements at a different frequency. The frequency of measurements ranged from many times a second (e.g.,

Table 2. Aircraft Data From the PHOBEA Experiment, Segregated by Back Trajectory Type and Altitude[a]

	NO			NO_x[b]			$J(NO_2)$, s^{-1}			Ozone, ppbv			PAN		
	All Marine	WNW	SW	All Marine	WNW	SW	All Marine	WNW	SW	All Marine	WNW	SW	All Marine	WNW	SW
0-2 km															
Average	12.6	10.9	1.6	35.9	31.9	6.6	0.0094	0.0086	0.0131	47	50	32	79	91	11
s.d. (1σ)	10.7	5 3	5.8	33.1	14.7	12.3	0 0032	0.0027	0.0017	10	6	17	68	72	2
Median	10.3	10.3	-1.2	30.2	32.4	0.6	0.0093	0.0090	0.0129	49	50	25	72	90	11
Maximum	42.7	25.2	10.3	160.8	61.4	25.0	0.0153	0.0132	0 0153	64	64	57	259	259	14
Minimum	-1.6	3.5	-1.6	0.3	9 0	0.3	0.0021	0.0017	0.0114	21	36	21	9	9	9
N_{ind}	26	22	4	26	22	4	26	22	4	28	24	4	22	16	3
N_{min}	288	226	35	282	225	35	622	455	78	655	504	78	79	53	12
2-4 km															
Average	12 5	12.7	11.9	23.7	24 8	21.3	0.0140	0.0133	0.0157	60	61	55	183	226	102
s.d (1σ)	6.0	6.9	3.8	12.9	14.4	8.9	0.0032	0 0024	0.0041	10	9	11	186	170	196
Median	11 1	10.6	11.5	20.7	21 2	18 7	0.0134	0.0123	0.0161	59	61	57	108	184	39
Maximum	28.4	28.4	19.1	52 0	52.0	37.3	0.0225	0 0175	0.0225	79	79	67	622	622	621
Minimum	4.3	4.3	6.0	7.0	7.0	8.6	0.0095	0 0095	0.0113	34	47	34	16	36	16
N_{ind}	30	21	9	30	21	9	30	21	9	31	22	9	26	17	9
N_{min}	305	207	98	305	207	98	667	442	215	691	466	215	91	52	39
4-6 km															
Average	12.5	14.0	9.4	20.5	22.4	14.4	0.0147	0 0148	0.0162	72	75	58	206	308	98
s d. (1σ)	7.9	10.8	4.0	15.9	22.0	6 8	0 0026	0.0013	0.0036	21	7	12	133	140	79
Median	10.7	10 7	7.7	18.3	13.6	11.4	0.0149	0.0151	0.0171	71	73	59	225	343	63
Maximum	37.3	37.3	14.3	70.1	70.1	22.1	0 0200	0.0159	0.0200	129	84	73	436	436	234
Minimum	5.2	6.7	5.2	6.8	7.7	6.8	0.0116	0.0121	0.0124	41	69	41	43	109	43
N_{ind}	15	7	5	15	7	5	15	7	5	12	4	5	12	4	5
N_{min}	186	96	53	186	96	53	418	206	130	354	142	130	62	27	22
6-8 km															
Average	12.9	14.4	6.6	18.8	18.6	8.7	0.0150	0.0156	0.0160	79	75	50	186	212	157
s d. (1σ)	5.9	5.8	3.4	10.0	6.4	4.1	0.0020	0.0017	0.0021	33	4	8	83	73	75
Median	13.6	14.1	5.3	17.4	16.8	7 1	0 0152	0.0153	0.0157	74	75	49	160	222	138
Maximum	25.0	25 0	11.6	39.6	29.8	14.8	0.0186	0.0181	0.0188	181	83	60	312	302	263
Minimum	4.1	8.1	4.1	5.7	12.0	5.7	0.0122	0.0128	0.0139	41	71	41	89	99	89
N_{ind}	14	7	4	14	7	4	14	7	4	15	8	4	13	6	4
N_{min}	194	108	55	194	108	55	354	193	99	357	196	99	51	25	16

	Ethane			Ethene			Ethyne			Propane		
	All Marine	WNW	SW	All Marine	WNW	SW	All Marine	WNW	SW	All Marine	WNW	SW
0-2 km												
Average	1.4	0.7	5.9	6.3	5.7	10 1	139	145	123	1.830	1.837	1.815
s.d. (1σ)	4.3	4.0	4.0	3.2	2 8	3.2	17	12	19	0.021	0.018	0.023
Median	2 1	2.1	7.3	6 3	5.7	11.3	146	146	121	1.839	1.839	1.812
Maximum	8 7	6.1	8.7	12.5	11 1	12.5	160	160	147	1.854	1.854	1 845
Minimum	-8.9	-8.9	0.1	0 5	0.5	5 4	103	115	103	1.790	1 792	1.790
N_{ind}	28	24	4	28	24	4	14	10	4	13	9	4
N_{min}	672	505	78	672	505	78	14	10	4	13	9	4
2-4 km												
Average	-8.4	-9.8	-4.8	2 0	1.8	2.4	139	149	123	1.824	1.838	1.812
s.d. (1σ)	7.6	6 9	8.6	1.4	1.3	1 4	29	13	40	0.026	0.006	0.030
Median	-8.3	-11.2	-3.3	1.9	2.0	1.8	144	152	114	1 832	1 837	1.815
Maximum	7.6	1.9	7 6	5.5	5 5	5.3	196	171	196	1.857	1.846	1 857
Minimum	-24 2	-24.2	-18.5	0 2	0.2	0 6	89	124	89	1.773	1.832	1.773
N_{ind}	32	23	9	32	23	9	15	9	6	11	5	6
N_{min}	719	494	215	719	494	215	15	9	6	11	5	6
4-6 km												
Average	20.3	-23.4	-14.8	1.1	0.8	2.1	132	144	95	1 801		1.790
s.d. (1σ)	5.8	5.0	3.8	0.9	0.4	0.6	26	9	3	0 036		0.029
Median	-19.9	-21 0	-13 8	1 1	0.8	2.1	145	146	95	1.792		1.790
Maximum	-10 6	-19.6	-10.6	2.7	1.4	2 7	158	152	97	1.847		1.811
Minimum	-32 2	-32 2	-19.9	0.1	0 2	1 4	93	135	93	1.770		1 770
N_{ind}	15	7	5	15	7	5	7	3	2	4		2
N_{min}	429	217	130	429	217	130	7	3	2	4		2
6-8 km												
Average	-32.3	-36 1	-25.4	0.5	0.4	1.1	130	135	104	1.827	1.827	
s.d. (1σ)	7.3	6.7	4.7	0.4	0.2	0 4	18	15		0.008	0 008	
Median	-31 0	-36.7	-26.0	0.3	0.3	1.1	132	135	104	1.825	1.825	
Maximum	-19.6	-27.5	-19.6	1.5	0.7	1.5	152	152	104	1.837	1.837	
Minimum	-48.3	-48.3	-30.0	0.1	0.1	0 7	104	108	104	1.820	1.820	
N_{ind}	17	10	4	17	10	4	7	6	1	4	4	
N_{min}	416	255	99	416	255	99	7	6	1	4	4	

Table 2. (continued)

	Temperature, °C			H_2O, ppthv			CO, ppbv			Methane, ppmv		
	All Marine	WNW	SW	All Marine	WNW	SW	All Marine	WNW	SW	All Marine	WNW	SW
0-2 km												
Average	1578	1727	1206	14.7	19.5	2.7	365	424	217	323	394	143
s.d. (1σ)	392	261	453	20.7	22.8	5.5	156	111	165	202	168	182
Median	1686	1744	1086	9.9	10.4	0	378	427	154	313	343	60
Maximum	2079	2079	1855	75.9	75.9	11.0	572	572	461	687	687	414
Minimum	799	1108	799	0	0	0	99	232	99	39	124	39
N_{ind}	14	10	4	14	10	4	14	10	4	14	10	4
N_{min}	14	10	4	14	10	4	14	10	4	14	10	4
2-4 km												
Average	1595	1900	1239	24.1	19.9	29.0	406	495	302	378	486	252
s.d. (1σ)	532	158	606	45.3	16.7	67 4	217	95	280	212	155	208
Median	1715	1913	1265	7.7	26.2	0	398	506	210	317	494	261
Maximum	2088	2079	2088	166.4	38.8	166.4	816	612	816	678	678	599
Minimum	499	1677	499	0	0	0	47	384	47	39	308	39
N_{ind}	13	7	6	13	7	6	13	7	6	13	7	6
N_{min}	13	7	6	13	7	6	13	7	6	13	7	6
4-6 km												
Average	1583	1979	1006	19.1	13.9	3.4	392	504	238	350	535	104
s d. (1σ)	583	295	460	23 1	12 2	5.9	172	8	165	234	79	89
Median	1629	1960	818	14 5	18 7	0	463	502	162	370	520	69
Maximum	2284	2284	1529	67.5	23.0	10.3	587	513	428	621	621	206
Minimum	669	1694	669	0	0	0	126	497	126	39	465	39
N_{ind}	8	3	3	8	3	3	8	3	3	8	3	3
N_{min}	8	3	3	8	3	3	8	3	3	8	3	3
6-8 km												
Average	1477	1582	849	25 4	25.8	23.1	337	360	199	288	324	76
s.d (1σ)	406	325		27 0	29 5		107	97		147	123	
Median	1634	1692	849	20.4	17.5	23.1	387	389	199	315	322	76
Maximum	1893	1893	849	83 1	83.1	23.1	431	431	199	449	449	76
Minimum	849	1000	849	0	0	23.1	173	173	199	76	107	76
N_{ind}	7	6	1	7	6	1	7	6	1	7	6	1
N_{min}	7	6	1	7	6	1	7	6	1	7	6	1

	n-Butane			i-Butane			n-Pentane			i-Pentane		
	All Marine	WNW	SW	All Marine	WNW	SW	All Marine	WNW	SW	All Marine	WNW	SW
0-2 km												
Average	72	91	24	40	49	18	7.9	9 4	4 2	9.2	11 1	4.5
s d (1σ)	60	57	36	35	35	22	5 6	6.1	0 7	7.5	8.3	1 1
Median	47	72	6	28	31	7	5 4	5.8	4.1	5.8	8 3	4 4
Maximum	200	200	78	117	117	51	21 1	21.1	5.2	29 1	29.1	5.8
Minimum	6	41	6	7	8	7	3.6	4.0	3.6	3.5	3 5	3.5
N_{ind}	14	10	4	14	10	4	14	10	4	14	10	4
N_{min}	14	10	4	14	10	4	14	10	4	14	10	4
2-4 km												
Average	91	118	60	54	72	34	13 3	12 1	14.6	13 9	17.5	9 7
s.d. (1σ)	64	61	58	40	36	36	16.2	6.0	24 1	11.4	12.3	9.5
Median	85	118	47	47	74	21	7.5	10 7	4.4	9 0	15.6	7 9
Maximum	196	196	151	115	115	100	62 1	20.4	62.1	33.9	33.9	26 9
Minimum	6	47	6	7	28	7	0	5.9	0	0	3.8	0
N_{ind}	13	7	6	13	7	6	13	7	6	13	7	6
N_{min}	13	7	6	13	7	6	13	7	6	13	7	6
4-6 km												
Average	85	139	22	54	90	7	10.0	14.8	5.3	13.8	17.2	15.2
s.d. (1σ)	64	20	23	48	15	0	6.1	2 9	6.3	7.2	3.3	9.8
Median	87	131	12	50	88	7	11 9	15.6	3 8	15.4	16.8	17.1
Maximum	161	161	49	117	106	7	17.1	17.1	12.2	23.9	20.6	23.9
Minimum	6	125	6	7	77	7	0	11 6	0	4.6	14.1	4.6
N_{ind}	8	3	3	8	3	3	8	3	3	8	3	3
N_{min}	8	3	3	8	3	3	8	3	3	8	3	3
6-8 km												
Average	60	69	7	39	41	27	13.5	15.1	3.7	32.9	36.4	12.1
s.d. (1σ)	38	33		19	20		10 3	10.2		27.1	28.0	
Median	67	69	7	41	44	27	12.8	14.6	3.7	33.9	40.0	12.1
Maximum	103	103	7	67	67	27	28.2	28 2	3.7	66 9	66.9	12.1
Minimum	7	11	7	7	7	27	3 5	3.5	3 7	0	0	12.1
N_{ind}	7	6	1	7	6	1	7	6	1	7	6	1
N_{min}	7	6	1	7	6	1	7	6	1	7	6	1

Table 2. (continued)

	Benzene			Toluene			$MeONO_2$			$EtONO_2$		
	All Marine	WNW	SW	All Marine	WNW	SW	All Marine	WNW	SW	All Marine	WNW	SW
0-2 km												
Average	60	65	46	14	15	12	4.2	4 6	3.2	4.3	4.7	3.4
s.d. (1σ)	54	57	47	19	21	17	1.3	1.2	0 7	1.3	0.9	1.8
Median	25	27	24	0	0	7	3.9	4.4	3.1	4.4	4.7	3 0
Maximum	160	160	117	49	49	35	7.3	7.3	4.0	6.3	6.3	6.0
Minimum	20	22	20	0	0	0	2.5	3.2	2.5	1 8	3.0	1.8
N_{ind}	14	10	4	14	10	4	14	10	4	14	10	4
N_{mn}	14	10	4	14	10	4	14	10	4	14	10	4
2-4 km												
Average	107	117	96	34	33	34	3 1	3.4	2.9	4.2	4 7	3.7
s.d. (1σ)	71	56	90	28	25	33	0.9	0 9	0.8	1.7	1.4	2.1
Median	98	142	78	28	43	25	3.1	3.6	2.6	5.0	5.1	3.4
Maximum	266	172	266	96	58	96	4.6	4.6	4.3	6.9	5.8	6.9
Minimum	24	24	24	0	0	0	1.7	1.7	2.0	1.7	1.8	1.7
N_{ind}	13	7	6	13	7	6	13	7	6	13	7	6
N_{mn}	13	7	6	13	7	6	13	7	6	13	7	6
4-6 km												
Average	190	186	256	47	72	42	3.0	3 6	2.3	3.7	5.3	2.4
s.d. (1σ)	172	101	280	47	55	49	0.8	0.8	0 2	1.7	1.1	1.0
Median	124	135	127	30	56	31	2.7	3.6	2.4	3.9	5.5	2.1
Maximum	578	302	578	134	134	96	4.4	4.4	2.4	6.3	6.3	3.6
Minimum	64	121	64	0	27	0	2.1	2.9	2.1	1 6	4.2	1.6
N_{ind}	8	3	3	8	3	3	8	3	3	8	3	3
N_{mn}	8	3	3	8	3	3	8	3	3	8	3	3
6-8 km												
Average	73	66	117	19	16	40	3.2	3.2	3.4	4.5	4.9	2.4
s.d. (1σ)	46	46		18	17		0.8	0.8		3 8	4.1	
Median	71	56	117	18	14	40	3.0	3.0	3.4	3.0	3.8	2.4
Maximum	146	146	117	46	46	40	4.9	4.9	3.4	12 6	12.6	2.4
Minimum	26	26	117	0	0	40	2.6	2.6	3.4	1.4	1.4	2.4
N_{ind}	7	6	1	7	6	1	7	6	1	7	6	1
N_{mn}	7	6	1	7	6	1	7	6	1	7	6	1

	n-$PrONO_2$			i-$PrONO_2$			2-$BuONO_2$			MeCl		
	All Marine	WNW	SW	All Marine	WNW	SW	All Marine	WNW	SW	All Marine	WNW	SW
0-2 km												
Average	1.7	1.8	1.3	7.2	7.9	5.5	6.1	6.9	4.2	579	577	582
s.d. (1σ)	1.2	1.2	1.1	4.6	4.0	6.2	4.3	4.0	4.9	27	30	21
Median	1.3	1.5	0.8	6.0	6.8	2.9	5.7	6.4	2.2	587	577	588
Maximum	4.6	4.6	2.9	14.7	14.5	14.7	13.6	13.6	11.4	630	630	601
Minimum	0.4	0.4	0.6	1.3	2.8	1.3	0.6	0.6	0 9	536	536	552
N_{ind}	14	10	4	14	10	4	14	10	4	14	10	4
N_{mn}	14	10	4	14	10	4	14	10	4	14	10	4
2-4 km												
Average	2.1	2.4	1.8	9.0	10.1	7.6	6.9	8.7	4.9	580	577	583
s d. (1σ)	1.5	1.7	1.4	6.7	6.1	7.7	5.6	5.7	5.2	36	38	36
Median	1.9	3.1	1.5	10.0	13.5	6.0	7.0	11.3	3.7	563	563	570
Maximum	4.8	4.8	4.3	20 7	15.9	20.7	15.9	15.9	13.4	647	629	647
Minimum	0	0	0 5	0.4	0.4	0.9	0	0	0.3	530	530	554
N_{ind}	13	7	6	13	7	6	13	7	6	13	7	6
N_{mn}	13	7	6	13	7	6	13	7	6	13	7	6
4-6 km												
Average	2.4	3.1	2.6	7.6	14.4	3.2	5.7	11 6	1.9	577	546	591
s.d. (1σ)	1.7	2.4	1 4	6.9	7.1	2.3	7.6	10.6	0.9	36	26	18
Median	1.8	2 2	2.3	5.4	12 8	3.1	2.6	9.3	1.5	573	539	595
Maximum	5 8	5.8	4.1	22 0	22.0	5.6	23.2	23.2	2.9	634	574	608
Minimum	0.8	1.2	1 4	0.9	8.2	0 9	0 8	2.3	1.3	524	524	572
N_{ind}	8	3	3	8	3	3	8	3	3	8	3	3
N_{mn}	8	3	3	8	3	3	8	3	3	8	3	3
6-8 km												
Average	1.3	1.4	0.8	11.4	12.8	3 0	2.5	2.7	1.4	586	592	555
s.d. (1σ)	1 3	1.4		20 6	22.2		2.1	2.2		36	36	
Median	1.0	1.1	0 8	3.7	4.5	3.0	1.8	2.0	1.4	592	602	555
Maximum	3.9	3.9	0.8	57.9	57.9	3.0	5.5	5 5	1.4	633	633	555
Minimum	0	0	0 8	0.7	0.7	3 0	0	0	1.4	535	535	555
N_{ind}	7	6	1	7	6	1	7	6	1	7	6	1
N_{mn}	7	6	1	7	6	1	7	6	1	7	6	1

Table 2. (continued)

	MeI			CH_2Br_2			CCl_4			CFC-11		
	All Marine	WNW	SW	All Marine	WNW	SW	All Marine	WNW	SW	All Marine	WNW	SW
0-2 km												
Average	0.65	0.77	0.37	1.82	1.90	1.61	121	121	122	293	292	298
s.d. (1σ)	0.68	0.78	0.08	0.23	0.21	0.11	7	7	6	12	13	12
Median	0.43	0.58	0.39	1.76	1.88	1.63	124	124	124	300	298	302
Maximum	2.92	2.92	0.46	2.25	2.25	1.72	127	127	126	306	304	306
Minimum	0.26	0.27	0 26	1.45	1.64	1.45	110	110	112	276	276	280
N_{ind}	14	10	4	14	10	4	14	10	4	14	10	4
N_{mun}	14	10	4	14	10	4	14	10	4	14	10	4
2-4 km												
Average	0 39	0.37	0.42	1.55	1.67	1.41	113	111	116	284	283	285
s.d. (1σ)	0.25	0.24	0.29	0.26	0.26	0.20	7	7	6	12	14	12
Median	0 42	0 42	0.37	1.61	1.69	1.40	111	111	113	277	275	279
Maximum	0.94	0.71	0.94	2 12	2.12	1.68	124	123	124	306	306	303
Minimum	0	0	0.16	1.13	1 24	1 13	99	99	110	273	273	275
N_{ind}	13	7	6	13	7	6	13	7	6	13	7	6
N_{mun}	13	7	6	13	7	6	13	7	6	13	7	6
4-6 km												
Average	0.32	0 38	0 29	1.54	1.61	1 42	113	108	115	280	271	285
s d. (1σ)	0 08	0.05	0 07	0.30	0 10	0.24	7	5	7	13	6	13
Median	0.34	0.38	0 26	1 56	1 66	1.52	111	108	112	276	271	278
Maximum	0 44	0.44	0 38	2 08	1.67	1 59	124	113	123	301	277	300
Minimum	0.20	0 33	0 24	1 14	1.49	1 14	103	103	111	265	265	276
N_{ind}	8	3	3	8	3	3	8	3	3	8	3	3
N_{mun}	8	3	3	8	3	3	8	3	3	8	3	3
6-8 km												
Average	0.27	0.27	0 28	1.59	1 66	1 20	117	117	113	289	291	278
s d. (1σ)	0.17	0.18		0 35	0.34		7	7		15	16	
Median	0.21	0 20	0 28	1.60	1 69	1.20	120	121	113	297	299	278
Maximum	0 61	0.61	0 28	2.03	2.03	1 20	124	124	113	303	303	278
Minimum	0 09	0 09	0.28	1.13	1.13	1.20	105	105	113	267	267	278
N_{ind}	7	6	1	7	6	1	7	6	1	7	6	1
N_{mun}	7	6	1	7	6	1	7	6	1	7	6	1

	CFC-12			$MeCCl_3$			CFC-113			CFC-114		
	All Marine	WNW	SW	All Marine	WNW	SW	All Marine	WNW	SW	All Marine	WNW	SW
0-2 km												
Average	581	578	588	65	66	64	85	86	83	14 66	14 69	14.60
s d (1σ)	35	38	31	4	4	2	5	6	3	0 45	0 49	0 37
Median	602	602	602	65	65	64	82	85	82	14 89	15.00	14 55
Maximum	614	614	605	78	78	66	97	97	88	15 23	15 23	15.02
Minimum	531	531	541	61	61	61	80	80	81	14.06	14.06	14.28
N_{ind}	14	10	4	14	10	4	14	10	4	14	10	4
N_{mun}	14	10	4	14	10	4	14	10	4	14	10	4
2-4 km												
Average	556	553	559	63	64	63	86	87	86	14.72	14 70	14.75
s.d. (1σ)	33	36	32	2	3	2	4	5	3	0.28	0.27	0 33
Median	538	534	540	63	63	63	87	87	87	14.80	14.75	14.85
Maximum	610	610	602	67	67	67	95	95	89	15.01	15 01	14.97
Minimum	528	528	537	59	59	60	81	81	81	14.11	14.17	14 11
N_{ind}	13	7	6	13	7	6	13	7	6	13	7	6
N_{mun}	13	7	6	13	7	6	13	7	6	13	7	6
4-6 km												
Average	549	528	557	63	64	62	88	91	88	14.48	14 48	14 59
s.d. (1σ)	34	9	37	3	5	2	5	5	6	0.27	0 13	0.45
Median	535	528	539	63	63	63	88	93	90	14.43	14 49	14 56
Maximum	606	536	600	69	69	63	93	93	92	15 05	14.60	15.05
Minimum	519	519	534	60	60	60	81	85	81	14 15	14 35	14 15
N_{ind}	8	3	3	8	3	3	8	3	3	8	3	3
N_{mun}	8	3	3	8	3	3	8	3	3	8	3	3
6-8 km												
Average	573	580	535	65	65	62	86	85	91	14.37	14.34	14.55
s.d. (1σ)	40	39		6	7		7	7		0 22	0.22	
Median	600	602	535	64	64	62	82	82	91	14 38	14 34	14 55
Maximum	609	609	535	73	73	62	98	98	91	14 65	14.65	14.55
Minimum	523	523	535	57	57	62	80	80	91	14.02	14.02	14.55
N_{ind}	7	6	1	7	6	1	7	6	1	7	6	1
N_{mun}	7	6	1	7	6	1	7	6	1	7	6	1

Table 2. (continued)

	C_2Cl_4			H1211			H2402			Aerosol CPC, number cm^{-3}		
	All Marine	WNW	SW	All Marine	WNW	SW	All Marine	WNW	SW	All Marine	WNW	SW
0-2 km												
Average	8.9	9.7	7.1	4.4	4.4	4.6	0.59	0.59	0.60	481	505	277
s.d. (1σ)	2.4	2.0	2.8	0.4	0.4	0.3	0.05	0.05	0.05	431	454	101
Median	9.1	9.6	6.3	4.5	4.5	4.5	0.62	0.61	0.62	360	440	265
Maximum	13.1	13.1	11.1	5.0	4.9	5.0	0.64	0.64	0.62	2129	2129	407
Minimum	4.9	7.2	4.9	3.8	3.8	4.2	0.52	0.52	0.53	75	75	172
N_{ind}	14	10	4	14	10	4	14	10	4	28	24	4
N_{min}	14	10	4	14	10	4	14	10	4	664	497	78
2-4 km												
Average	9.1	10.4	7.6	4.5	4.3	4.8	0.54	0.55	0.54	544	611	372
s.d. (1σ)	3.7	2.0	4.9	0.5	0.6	0.3	0.04	0.05	0.04	528	601	202
Median	9.1	11.4	6.1	4.7	4.1	4.8	0.52	0.52	0.52	375	421	262
Maximum	16.1	12.5	16.1	5.5	5.5	5.2	0.64	0.64	0.60	2774	2774	799
Minimum	3.4	7.9	3.4	3.8	3.8	4.4	0.49	0.49	0.51	33	33	192
N_{ind}	13	7	6	13	7	6	13	7	6	32	23	9
N_{min}	13	7	6	13	7	6	13	7	6	712	488	215
4-6 km												
Average	8.3	12.4	4.5	4.6	4.3	4.9	0.53	0.51	0.54	467	543	363
s.d. (1σ)	4.7	5.2	1.5	0.5	0.6	0.5	0.05	0.01	0.06	145	168	88
Median	7.7	9.7	5.2	4.5	4.1	4.8	0.51	0.51	0.51	451	540	412
Maximum	18.3	18.3	5.5	5.5	5.0	5.5	0.62	0.52	0.61	815	815	446
Minimum	2.8	9.1	2.8	3.9	3.9	4.5	0.49	0.49	0.50	248	304	248
N_{ind}	8	3	3	8	3	3	8	3	3	14	6	5
N_{min}	8	3	3	8	3	3	8	3	3	393	190	130
6-8 km												
Average	9.2	10.0	4.3	4.7	4.7	4.7	0.58	0.59	0.51	508	595	389
s.d. (1σ)	4.7	4.5		0.5	0.5		0.06	0.05		192	195	147
Median	9.6	9.9	4.3	4.7	4.8	4.7	0.60	0.61	0.51	476	567	341
Maximum	15.9	15.9	4.3	5.4	5.4	4.7	0.64	0.64	0.51	980	980	603
Minimum	4.3	4.3	4.3	4.0	4.0	4.7	0.51	0.52	0.51	273	412	273
N_{ind}	7	6	1	7	6	1	7	6	1	16	9	4
N_{min}	7	6	1	7	6	1	7	6	1	375	229	84

	Aerosol σ_{ap}, $x10^{-6}$ m^{-1}			Aerosol σ_{sb}, $x10^{-6}$ m^{-1}			Aerosol σ_{sg}, $x10^{-6}$ m^{-1}			Aerosol σ_{st}, $x10^{-6}$ m^{-1}		
	All Marine	WNW	SW	All Marine	WNW	SW	All Marine	WNW	SW	All Marine	WNW	SW
0-2 km												
Average	0.21	0.18	0.57	3.3	3.3	4.1	2.2	2.2	2.7	1.4	1.4	1.6
s.d. (1σ)	0.20	0.21	0.53	2.3	2.4	3.1	1.6	1.7	2.1	1.0	1.1	1.2
Median	0.16	0.12	0.37	3.5	3.8	3.4	2.5	2.5	2.1	1.5	1.5	1.3
Maximum	0.68	0.68	1.34	8.1	8.1	8.3	5.4	5.4	5.6	3.4	3.4	3.3
Minimum	-0.18	-0.18	0.21	0.0	0.0	1.2	-0.1	-0.1	0.9	0.1	0.1	0.6
N_{ind}	28	24	4	28	24	4	28	24	4	28	24	4
N_{min}	600	458	66	664	497	78	664	497	78	664	497	78
2-4 km												
Average	0.73	0.58	1.11	7.2	6.4	9.2	4.8	4.1	6.4	2.8	2.4	4.1
s.d. (1σ)	0.72	0 68	0.71	7.8	8.1	6.9	5.3	5.4	4.8	3.0	3.0	3.0
Median	0.49	0.30	1.03	3.8	3.7	6.7	2.5	2.0	4.6	1.6	1.3	2.6
Maximum	2.62	2.62	2.59	31.0	31.0	20.7	21.0	21.0	14.0	11.9	11.9	8.2
Minimum	-0.20	-0.20	0.48	-0.1	-0.1	2.3	-0.1	-0.1	1.6	0.0	0.0	1.1
N_{ind}	32	23	9	32	23	9	32	23	9	32	23	9
N_{min}	623	432	190	712	488	215	712	488	215	712	488	215
4-6 km												
Average	0.88	0.68	0.99	10.2	7.9	11.0	7.0	5.3	7.8	4.2	3.0	4.7
s.d. (1σ)	0.78	0.77	1.03	10.2	9.9	13.5	7.0	6.6	9.6	4.2	3.6	5.7
Median	0.65	0.43	0.45	6.9	3.8	3.6	4.6	2.6	2.7	2.8	1.5	1.7
Maximum	2.72	1.88	2.72	33.4	26.5	33.4	23.6	17.4	23.6	14.0	9.5	14.0
Minimum	-0.06	-0.06	0.24	0.8	0.8	1.9	0.4	0.4	1.1	0.2	0.2	0.5
N_{ind}	14	6	5	14	6	5	14	6	5	14	6	5
N_{min}	307	155	105	393	190	130	393	190	130	393	190	130
6-8 km												
Average	0.54	0.55	0.47	5.8	5.9	4.1	3.8	3.9	2.6	2.1	2.2	1.4
s.d. (1σ)	0.39	0.38	0.46	3.7	3.1	4.1	2.5	2.1	2.7	1.5	1.2	1.4
Median	0.49	0.51	0.31	5.1	6.2	2.2	3.4	4.0	1.4	2.0	2.1	0.7
Maximum	1.19	1.13	1.13	13.3	10.6	10.3	9.3	7.3	6.7	5.6	4.3	3.4
Minimum	-0.02	-0.02	0.13	1.1	1.1	1.9	0.7	0.7	1.1	0.4	0.4	0.5
N_{ind}	16	9	4	16	9	4	16	9	4	16	9	4
N_{min}	333	209	75	375	229	84	375	229	84	375	229	84

Table 2. (continued)

	Aerosol σ_{bsb}, x10^{-6} m^{-1}			Aerosol σ_{bsg}, x10^{-6} m^{-1}			Aerosol σ_{bsr}, x10^{-6} m^{-1}		
	All Marine	WNW	SW	All Marine	WNW	SW	All Marine	WNW	SW
0-2 km									
Average	0.20	0.19	0.36	0.05	0.04	0.12	-0.02	-0.03	0.06
s.d. (1σ)	0.21	0.22	0.19	0.16	0.16	0.14	0.11	0.12	0.04
Median	0.16	0.17	0.34	0.01	0.05	0.12	-0.04	-0.07	0.06
Maximum	0.59	0.59	0.58	0.36	0.36	0.26	0.18	0.18	0.10
Minimum	-0.24	-0.24	0.16	-0.21	-0 21	0.00	-0.25	-0.25	0.02
N_{ind}	28	24	4	28	24	4	28	24	4
N_{min}	664	497	78	664	497	78	664	497	78
2-4 km									
Average	0.65	0.57	0.86	0.45	0.38	0.63	0.31	0.26	0.45
s.d. (1σ)	0 76	0.81	0.64	0.60	0.62	0.52	0.45	0.46	0.40
Median	0.38	0 28	0 79	0.24	0.11	0.60	0.17	0.12	0.46
Maximum	2.88	2.88	1.91	2.05	2.05	1.57	1.51	1.51	0.99
Minimum	-0.31	-0.31	0.15	-0.24	-0.24	0.12	-0.24	-0.24	-0.05
N_{ind}	32	23	9	32	23	9	32	23	9
N_{min}	712	488	215	712	488	215	712	488	215
4-6 km									
Average	1.03	0.81	1.07	0 77	0 58	0.84	0 59	0.40	0.65
s.d (1σ)	0 90	0.84	1 20	0.73	0.74	0.93	0 57	0.61	0 66
Median	0.72	0.46	0.43	0 63	0.38	0.32	0.50	0.20	0.33
Maximum	2.97	2.31	2.97	2 37	1.93	2.37	1 78	1.51	1 78
Minimum	0.14	0.14	0.17	-0.05	-0.05	0.17	-0.12	-0.12	0.12
N_{ind}	14	6	5	14	6	5	14	6	5
N_{min}	393	190	130	393	190	130	393	190	130
6-8 km									
Average	0 80	0.71	0.81	0 65	0 65	0.56	0 55	0 51	0 53
s d. (1σ)	0.30	0.28	0.34	0.29	0 24	0 28	0 24	0 23	0.18
Median	0.79	0 69	0.86	0 68	0.72	0 57	0 63	0.61	0 54
Maximum	1.47	1.10	1 17	1.35	0.94	0.89	1 00	0.73	0 72
Minimum	0 36	0 20	0 36	0.22	0.22	0 22	0.16	0.14	0 34
N_{ind}	16	9	4	16	9	4	16	9	4
N_{min}	375	229	84	375	229	84	375	229	84

[a]WNW and SW data have been screened to remove local boundary layer pollution cases (99 out of a total 2236 min) and stratospheric intrusions (144 out of 2236 min) as described in the text. N_{ind} are the number of statistically independent measurements; N_{min} are the number of measured 1-min averages. Mixing ratios are in pptv unless otherwise noted All aerosol measurements were adjusted to their values at STP. [b]NO_x is calculated from the Leighton relationship as described in the text

temperature), to once every 5 min (e.g., PAN), to a few times over the course of a flight (e.g., VOCs). These were consolidated into a master file of 1-min averages. We present in Table 2 a summary of all marine data (i.e., excluding the one continental North American air mass) and two subsets of the marine data: WNW and SW where both subsets were screened to remove local pollution and stratospheric sources as discussed above. Unless otherwise noted, mixing ratios in Table 2 are in pptv, N_{min} represents the number of measured 1-min averages, and N_{ind} denotes the number of 20-min flight legs making up the average, which better approximates the number of statistically independent samples.

3.5. Comparing WNW With SW Data

The WNW and SW data are compared by evaluating the level of significance (LOS) between the average mixing ratios at the same altitude. The LOS was computed from equations (1)-(3)

$$\mathrm{LOS} = 1 - \mathrm{TDIST}_{t,df,2} \tag{1}$$

$$t = \left| \frac{\overline{X}_{SW} - \overline{X}_{WNW}}{\sqrt{\frac{(N_{SW}-1)\sigma_{SW}^2 + (N_{WNW}-1)\sigma_{WNW}^2}{df}}\sqrt{\frac{1}{N_{SW}} + \frac{1}{N_{WNW}}}} \right| \tag{2}$$

$$df = N_{SW} + N_{WNW} - 2 \tag{3}$$

where $\mathrm{TDIST}_{t,df,2}$ is the value of the two-sided student's t distribution, t is the value of the t statistic as defined above, df is the number of degrees of freedom, $\overline{X}_{SW}$ and $\overline{X}_{WNW}$ are the average mixing ratio of a species during SW and WNW regimes, respectively, N_{SW} and N_{WNW} are the number of 20-min flight legs in each trajectory regime, and σ_{SW} and σ_{WNW} are the standard deviation of the leg-averaged measurements in each trajectory regime.

The LOS values listed in Table 3 indicate the confidence level at which the difference in average mixing ratio becomes significant (e.g., a LOS equal to 0.95 would indicate a difference in average mixing ratio between species in the SW and WNW regimes significant at the 95% confidence level). Missing LOS values indicate less than two independent measurements in either WNW or SW regimes. The LOS averaged over all altitudes is also presented. It is important to note that an LOS analysis assumes that the data are normally distributed. For those data that were significantly skewed, LOSs were also computed from the lognormal distributions. However, the LOSs from the lognormal distributions did not differ significantly from those listed in Table 3, therefore we report only LOSs from the measured distributions.

Numerous species show significantly enhanced mixing ratios in WNW back trajectories when compared to SW back trajectories. We can explain these enhanced mixing ratios by examining the factors which influence the concentrations of species measured. These factors are as follows: the back-

Table 3. Statistical Level of Significance (LOS) Between Species Measured in WNW and SW Back Trajectories, Delineated by Altitude[a]

Species	LOS, 0-2 km	LOS, 2-4 km	LOS, 4-6 km	LOS, 6-8 km	LOS, Average
NO	(1.00)	0.25	0.61	(0.96)	0.70
NO_x[b]	(1.00)	0.49	0.55	(0.98)	0.75
$J(NO_2)$	(1.00)	(0.95)	0.65	0.32	0.73
Ozone	(1.00)	(0.90)	(0.96)	(1.00)	(0.96)
PAN	(0.92)	(0.89	(0.98)	0.72	(0.88)
Temperature	(0.98)	(0.91)	(0.99)	(0.99)	(0.97)
H_2O	(0.99)	0.68	(1.00)	(1.00)	(0.92)
CO	(0.98)	(0.91)	(1.00)		(0.96)
Methane	(0.92)	(0.91)			(0.91)
Ethane	(0.98)	(0.98)	(0.96)		(0.98)
Ethene	(0.82)	0.27	0 75		0.61
Ethyne	(0.98)	(0.89)	(0.95)		(0.94)
Propane	(0.97)	(0.96)	(1.00)		(0.98)
n-Butane	(0.95)	(0.89)	(1.00)		(0.95)
i-Butane	(0.87)	(0.92)	(1.00)		(0.93)
n-Pentane	(0.88)	0.21	(0.92)		0.67
i-Pentane	(0.85)	0.77	0.24		0.62
Benzene	0.43	0.39	0.30		0.37
Toluene	0.18	0.06	0.48		0.24
$MeONO_2$	(0.95)	0.67	(0.96)		(0.86)
$EtONO_2$	(0.90)	0.65	(0.97)		(0.84)
n-$PrONO_2$	0.56	0.53	0.22		0.44
i-$PrONO_2$	0.60	0 47	(0.94)		0.67
2-$BuONO_2$	0.71	0.77	(0.81)		0.76
MeCl	0.24	0.23	(0.93)		0.46
MeI	0.65	0.26	(0.83)		0.58
CH_2Br_2	(0.97)	(0.93)	0.72		(0.87)
CCl_4	0.21	0.75	0.79		0.58
CFC-11	0.56	0 26	(0.82)		0.55
CFC-12	0.33	0.23	0.76		0.44
$MeCCl_3$	0.66	0.25	0.40		0.44
CFC-113	0.66	0 23	0.44		0.44
CFC-114	0.24	0.24	0.29		0.26
C_2Cl_4	(0.92)	(0.81)	(0.94)		(0.89)
H1211	0.59	(0.89)	0.75		0.74
H2402	0.25	0.12	0.62		0.33
Aerosol CPC	0.67	0.74	(0.94)	(0.91)	(0.82)
Aerosol σ_{ap}	(0.99)	(0.94)	0.42	0.26	0.65
Aerosol σ_{sb}	0.42	0.62	0.33	0.60	0.49
Aerosol σ_{sg}	0.40	0.73	0.37	0.63	0.53
Aerosol σ_{sr}	0.30	(0.85)	0.43	0.70	0.57
Aerosol σ_{bvb}	(0.82)	0.66	0.32	0.42	0.56
Aerosol σ_{bsg}	0.63	0.71	0.37	0.40	0.53
Aerosol σ_{bsr}	(0.86)	0.72	0.48	0.12	0.54

[a]LOSs in parentheses are those values greater than or equal to 0.80. The average over all altitudes is also calculated. No data indicates less than two independent measurements in either WNW or SW regimes.
[b]NO_x is calculated from the Leighton relationship as described in the text.

ground latitudinal gradient of the species, its lifetime in the troposphere, East Asian continental emissions relative to the background, and the typical transport pathway across the Pacific during the study. However, these factors are not independent of one another.

Increasing actinic flux and temperature with decreasing latitude shortens the lifetime of most trace gases at lower latitudes. Those compounds with lifetimes of the order of or less than the latitudinal mixing time (approximately months) will have stronger latitudinal gradients. Those compounds with long lifetimes relative to the latitudinal mixing time will have weak latitudinal gradients.

East Asian continental emissions influence the latitudinal gradient of trace species in the Pacific in several ways. First, they contribute to the overall tropospheric concentration over the Pacific. However, this contribution is not uniform with latitude; the largest input of East Asian continental emissions comes from the midlatitudes [*Blake et al.*, 1997]. Second, we have shown that during the experimental period, fast transport across the Pacific from midlatitude Asian sources favored transport to latitudes higher than 40°N.

The vertical gradient observed during NASA's PEM-West B experiment in 1994 provides a measure of the East Asian continental signal. Those species with the strongest signal, in general, have the greatest likelihood of being detected in the northeastern Pacific. Strongly negative vertical gradients (high values at the surface and lower values aloft) were measured during PEM-West B for CO, MeI, ethane, ethene, C_2Cl_4, ethyne, propane, i-pentane, n-pentane, i-butane, n-butane, benzene, PAN, and aerosol CPC [*Talbot et al.*, 1997]. Many of the species in this list (CO, ethane, C_2Cl_4, ethyne, propane, i-butane, n-butane, PAN, and aerosol CPC) have a high average LOS between mixing ratios measured in the WNW and SW regimes, WNW mixing ratios being significantly higher. However, the average LOS for MeI was low, reflecting that its primary source is oceanic. The average LOSs for i-pentane, n-pentane, and ethene were also low, reflecting that their lifetimes are short (~1-3 days assuming an average OH con-

centration of $1x10^6$ molecules cm^{-3}) compared to the others and are significantly shorter than the average transport time across the Pacific (~10 days). Hence the lifetime is short enough that Asian continental emissions likely do not survive transport in either WNW or SW regimes to any great degree. The only remaining species, benzene, had a low average LOS, which was inconsistent with the high LOSs of the other anthropogenically produced trace gases of similar lifetime. PAN mixing ratios are higher in the WNW regime due to lower temperatures that result in slower losses, and high PAN may also explain the elevated NO_x mixing ratios in the WNW regime. Aerosol number concentrations were also somewhat higher in WNW trajectories. SW back trajectories are likely more remote from anthropogenic sources, hence there is a longer time period for cloud and depositional processes to reduce the aerosol number concentration relative to air masses with WNW back trajectories.

Enhanced mixing ratios in WNW trajectories of those species with a high LOS cannot be a priori attributed to East Asian emissions. These higher mixing ratios likely reflect the combined influences of latitudinal gradient and faster transport of Asian continental emissions to the WNW region.

Apart from the patterns in LOS discussed above, moderate to strong differences were also seen in NO_x (average LOS equal to 0.75), ozone (average LOS equal to 0.96), and $J(NO_2)$ (average LOS equal to 0.73).

NO_x mixing ratios were higher in air masses with WNW back trajectories. NO_x has its primary source in urban areas and has a lifetime of less than 1 day in the lower troposphere and 4-7 days in the upper troposphere [*Brasseur et al.*, 1999]. Therefore it is unlikely that direct anthropogenic emissions from the East Asian region influenced our measurements in the lower troposphere. As mentioned above, higher PAN mixing ratios in the WNW regime likely play some role in elevating NO_x mixing ratios. However, while we have attempted to screen our data from the direct effects of ship emissions, the effects of older diffuse emissions in our boundary layer data cannot be discounted [*Corbett et al.*, 1999].

Ozone mixing ratios were significantly lower in air masses with SW back trajectories. Ozone production rates should be lower in the SW regime due to lower NO_x mixing ratios, and ozone destruction rates should be higher due to increased actinic fluxes at lower latitudes and higher water vapor concentrations. Additionally, the SW region is less subject to intrusions of ozone from the stratosphere [*Elbern et al.*, 1998]. While we have attempted to remove the effects of recent stratospheric intrusions, we cannot account for older intrusions that have become well mixed into the background. These likely play some role in enhancing ozone in the WNW regime.

$J(NO_2)$ was higher in air masses with SW back trajectories because synoptic conditions leading to SW flow were generally associated with high pressure in Oregon and northern California and clearer skies, particularly at lower elevations. $J(NO_2)$ also tended to increase with height during all daytime flights mainly due to the effects of low-level clouds.

3.6. Comparing the Relative Photochemical Age of Air Masses With Their Trajectory Age

Hydrocarbon ratios can be used to estimate the age of an air mass from its source region [*Parrish et al.*, 1992; *Greenberg et al.*, 1996]. Assuming only photochemical loss from the second-order reaction with hydroxyl radical, Greenberg et al. derived equation (4) as the relative photochemical age t_r of an air mass

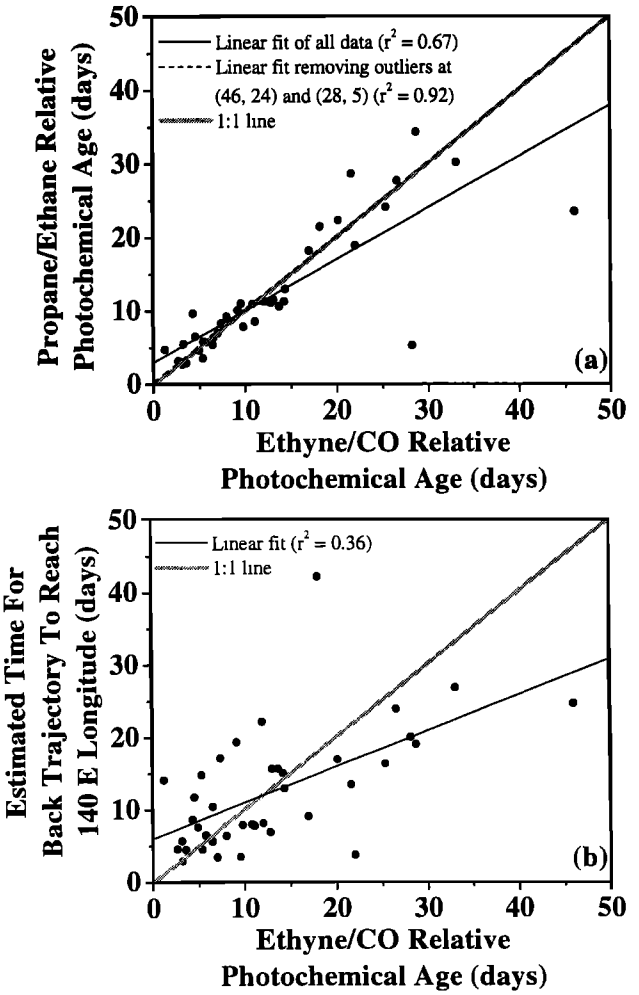

Figure 5. Relative photochemical age determined from the ethyne/CO ratio and plotted against (a) relative photochemical age determined from the propane/ethane ratio and (b) the estimated air mass age from back trajectories.

$$t_r = \{\ln([A]/[B]) - \ln([A]_0/[B]_0)\} / \{(k_B - k_A)[OH]_{average}\} \quad (4)$$

where $[A]/[B]$ is the measured ratio of hydrocarbons A and B, $[A]_0/[B]_0$ is the ratio of A and B in the source region, k_A and k_B are the second order rate constants for the reaction of A and B with OH, respectively, and $[OH]_{average}$ is the average OH concentration encountered by the air mass.

We calculated t_r for each VOC sample using the measured ratios of propane/ethane and ethyne/CO during PHOBEA and by using the following assumptions; source region concentrations were the average measured ratios from 0-2 km of propane/ethane and ethyne/CO during NASA's PEM-West B experiment [*Talbot et al.*, 1997], $[OH]_{average}$ was $1x10^6$ molecules cm^{-3}, and reaction rate constants were at STP. Figure 5a shows a plot of t_r from propane/ethane versus t_r from ethyne/CO for each VOC sample. There is generally good agreement. Linear regression gives a best fit of

$$t_{r(propane/ethane)} = (0.70\pm0.08)\, t_{r(ethyne/CO)} + (3.0\pm1.3) \quad (5)$$

with $r^2 = 0.67$. However, this regression is highly leveraged

Table 4. Air Mass Age Determined by Two Methods, Photochemical and Back Trajectory, and Delineated by Back Trajectory Type[a]

	Measured: PEM-West B	Measured: PHOBEA	
		WNW	SW
Ethyne/CO, pptv/ppbv	4.40±0.67	2.79±0.99	1.87±1.01
Propane/ethane, pptv/pptv	0.40±0.07	0.23±0.06	0.13±0.09
Photochemical age from ethyne/CO, days		9 9±8.4	18.7±12.3
Photochemical age from propane/ethane, days		7.9±4.6	16.2±15.1
Average age from back trajectories, days		8.1±4.6	19.6±5.1

[a]Photochemical age calculations assume hydrocarbon source ratios as measured during NASA's PEM-West B experiment, [OH] = $1x10^{-6}$ molecules cm^{-3}, and reaction rate constants at STP. Average age from back trajectories are the estimated time of flight from 140°E longitude to the measurement location off the coast of Washington State.

by two outliers; if the outliers at (46, 23) and (28,5) are removed, the regression becomes

$$t_{r(\text{propane/ethane})} = (1.00\pm0.05)\, t_{r(\text{ethyne/CO})} + (0.33\pm0.72) \quad (6)$$

with $r^2 = 0.92$, the slope and intercept lying statistically on the 1:1 line.

We also estimated the age of each air mass from the 5 day back isentropic trajectory data. To do this, we assumed that the source region was at 140°E longitude, then calculated the average eastward progress per day from the 5 day back trajectory and extrapolated to the time required to travel across the Pacific (i.e., from 140°E longitude to the measurement location off the west coast of Washington State). Figure 5b shows the trajectory estimated age versus t_r from ethyne/CO. The linear correlation of data in Figure 5b is poorer than that in Figure 5a, with linear regression $r^2 = 0.36$ and for the correlation of t_r from propane/ethane with the trajectory estimated age (which is not shown), $r^2 = 0.32$. This poorer agreement likely reflects errors associated with assuming that the eastward progress over 5 days matched that of the remaining transpacific crossing, the uncertainties in VOC mixing ratios, and the assumptions of constant pressure, temperature, and OH concentration.

Nonetheless, if the average age is calculated for each trajectory regime, then there is good agreement between the two methods. The average age estimated by each method and delineated by trajectory type is listed in Table 4. Each calculation estimates the average age to be roughly 8-10 days for air masses with WNW back trajectories and 16-20 days for air masses with SW back trajectories.

3.7. Comparing PHOBEA Data With That From NASA's PEM-West B Experiment

Figure 6 compares the PHOBEA WNW mixing ratios of PAN, CO, ethane, and propane with springtime measurements from NASA's PEM-West B experiment during 1994 in the northwestern Pacific. The median trace gas mixing ratios from the northwestern Pacific are those presented by *Kondo et al.* [1997] and *Talbot et al.* [1997], representing different latitudinal averages of the springtime Asian continental outflow. Kondo et al. present median values measured between 15°-40°N latitude, and Talbot et al. present median values measured north of 20°N latitude. By comparing the vertical profiles of median mixing ratios compiled by Kondo et al. and Talbot et al. (Figure 6) a latitudinal gradient of higher mixing ratios poleward is evident for CO, ethane, and propane in the Asian continental outflow. However, it is interesting to note that the median PAN mixing ratios were higher between 15°N-40°N than at more northern latitudes. This likely indicates a large source region for PAN between 15°N-40°N relative to higher latitudes.

The bowed shape of PAN, CO, ethane, and propane profiles in Figure 6 is consistent with long-range transport of anthropogenic trace gases from the northwestern Pacific. We surmise that the vertical profile of these trace gases in the springtime 1999 Asian continental outflow is at least qualitatively similar to that in 1994. Once boundary layer air mixes into the free troposphere over the northwestern Pacific, stronger westerly winds above the boundary layer can transport it more rapidly to the northeastern Pacific. The highest mixing ratios of these gases during PHOBEA were measured between 2-6 km. PHOBEA WNW mixing ratios from 0-2 km were lower than from 2-6 km because removal rates of these compounds are faster in the boundary layer. In addition, air masses measured between 0-2 km were slower in transit across the Pacific than those between 2-8 km. PHOBEA WNW mixing ratios from 6-8 km are also lower than those from 2-6 km likely because fewer air masses have mixed up to that height in their transport across the Pacific.

Table 5 compares the integrated column concentrations from 0-7 km of PAN, CO, ethane, and propane measured in the Asian continental outflow during PEM-West B and in the northeastern Pacific during PHOBEA. When comparing these data sets, it must be noted that they represent different years, 1994 versus 1999, and different latitude ranges. Each of these compounds is known to have had a strong latitudinal gradient, and the emissions rate of these compounds is likely to have changed somewhat over the 5 year time frame. Having said that, the column concentrations of these four species were in general larger during PEM-West B than in PHOBEA, which is consistent with photochemical removal and dilution with cleaner air masses during long-range transport.

3.8. Dominant Correlations

Table 6 presents the linear correlation matrix (r values) for selected species and includes those with a LOS greater than 0.9. In general, the correlations between VOCs are good, but they are poorly correlated with water vapor and ozone. Water vapor is primarily affected by air and sea surface temperatures, which increase with decreasing latitude, and ozone is a secondary pollutant, which is not expected to correlate with primary pollutants far from their source regions. Hence the poor correlation of VOCs with water vapor and ozone is not surprising.

The other major correlations were between aerosol scattering and absorption (but not with number concentration, which is not shown), with correlation coefficients ranging between 0.88 and 1.0. Aerosol scattering and absorption were

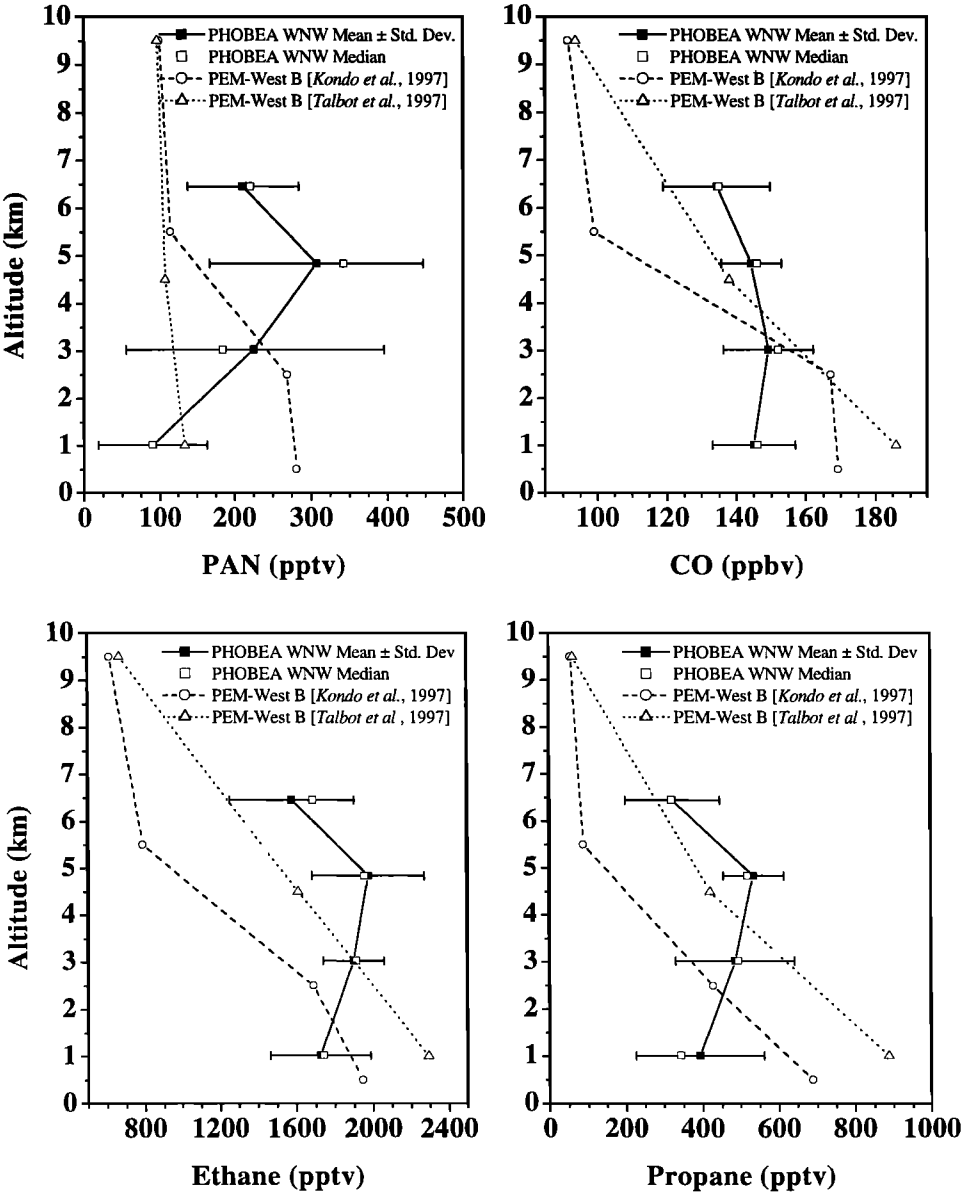

Figure 6. Four examples of PHOBEA aircraft data from the springtime northeastern Pacific in 1999, with local pollution and stratospheric sources removed (see text), plotted with two aircraft data sets from NASA's PEM-West B experiment from the springtime northwestern Pacific in 1994 [*Kondo et al.*, 1997; *Talbot et al.*, 1997].

also loosely correlated with PAN (r values ranging between 0.6 and 0.7). However, aerosol scattering and absorption were uncorrelated with the VOCs listed in Table 6. PAN, on the other hand, showed a moderate correlation with the VOCs (r values ranging between 0.6 and 0.7).

3.9. Implications of Transpacific Pollution Transport

In a previous publication we have shown that episodic transport events can bring enhanced concentrations of industrial pollutants from Asia to the northeastern Pacific within 5 days [*Jaffe et al.*, 1999]. In this report we use the PHOBEA aircraft data to show that industrial emissions from Asia influence the entire lower troposphere in the northeastern Pacific, not only in episodic transport events, but also in the background concentrations of ozone and other species observed. *Guderian et al.* [1985, and references therein] have shown that ozone mixing ratios as low as 35 ppbv can damage florae in controlled studies and that the damage to plant growth increases linearly with increasing ozone. The average marine mixing ratios of ozone in the PHOBEA aircraft measurements were 47 ppbv in the 0-2 km layer and 60 ppbv in the 2-4 km layer. Air masses at these altitudes likely encounter the florae of the Pacific northwest, where the highest mountain peaks can extend above 4 km (e.g., Mount Rainier at 4.4 km) and high alpine forests can range between 2 and 3 km. Hence it is possible that marine ozone from the northeastern Pacific has a detrimental impact on the biosphere of the northwestern United States and Canada. However, the issue is complicated because alpine florae may be adapted to higher ozone concentrations and the largest ozone impact on plants

Table 5. Column Concentrations of Four Pollution Tracers During NASA's PEM-West B Experiment in 1994 and During the PHOBEA Aircraft Experiment

Species	Column Concentrations Calculated From 0-7 km, 15°N-40°N Latitude, During PEM-West B,[a] $x10^{15}$ molecules cm^{-2}	Column Concentrations Calculated From 0-7 km, >20°N Latitude, During PEM-West B,[b] $x10^{15}$ molecules cm^{-2}	Column Concentrations Calculated From 0-7 km, 39°N-48°N Latitude, During PHOBEA, $x10^{15}$ molecules cm^{-2}
PAN	2.41	1.31	1.67
CO	1550	1750	1460
Ethane	15.8	21.0	18.1
Propane	4.23	6 86	4.14

[a]Derived from *Kondo et al.* [1997].
[b]Derived from *Talbot et al.* [1997].

occurs during the summer growing season, whereas our measurements were in the spring.

A modeling study by *Berntsen et al.* [1999] has shown that about 4 ppbv (roughly 10%) of the ozone in air arriving to North America during spring is due to current emissions of NO_x from Asia. As a result of continued rapid growth in NO_x emissions from China [*Streets and Waldhoff*, 2000] ozone in the northeastern Pacific is predicted to continue increasing [*Berntsen et al.*, 1999; *Jacob et al.*, 1999]. Other modeling studies have suggested that PAN transported from continental regions provides a significant contribution to NO_x in the northeastern Pacific through PAN's thermal decomposition [*Moxim et al.*, 1996; *Horowitz and Jacob*, 1999]. NO_x from PAN would help sustain higher ozone concentrations in air masses transported across the Pacific. In future publications we will employ a photochemical model constrained with the PHOBEA data to estimate the ozone photochemical tendency in the northeastern Pacific and explore the impacts of PAN thermal decomposition and increasing Asian NO_x emissions on ozone in the northeastern Pacific.

4. Concluding Remarks

In this paper we have presented the most comprehensive suite of aircraft measurements of trace gases and aerosols in the northeastern Pacific troposphere to date. The data are consistent with transport from the northwestern Pacific in 8-20 days. The impacts of this transpacific transport extend throughout the 0-8 km column.

After screening the data to remove local pollution and two cases of direct stratospheric input, the marine data were segregated into two regions based on 5 day back isentropic trajectories. The majority of these back trajectories, 71 of 93, originated north of 40°N latitude or west of 180°W longitude (termed westerly and northwesterly, WNW), and the remainder originated south of 40°N latitude and east of 180°W longitude (termed southwesterly, SW). The relative number of air masses with 5 day origin in the WNW and SW regions were consistent with climatology. Further trajectory analyses indicated that the majority of air from both regions was likely to have originated from the northwestern Pacific, without recent exposure to the North American continent.

Our aircraft measurements in the remote northeastern Pacific were compared with a similar set of measurements in the Asian continental outflow, made during NASA's PEM-West B experiment in the spring of 1994. In WNW air masses we observed elevated mixing ratios of anthropogenic hydrocarbons associated with East Asian emissions. Two methods were used to estimate the time since exposure to Asian emissions; VOC ratios and trajectory calculations. Both methods found an average age of air masses with WNW back trajectories of 8-10 days and the age of air masses with SW back trajectories of 16-20 days.

Appendix A: Instrumental Descriptions and Quality Control

A1. Ozone

Ozone was measured at aircraft cabin pressure with a Dasibi 1008 AH, which utilized UV absorption and compensated for pressure and temperature fluctuations. Air was brought in through a single 3/8 inch inner diameter (ID) Teflon-lined backward facing inlet for both O_3 and NO instruments (all inlets extended beyond the boundary layer of the aircraft). A metal bellows pump pulled air at approximately 17 L min^{-1} (at

Table 6. Linear Correlation Matrix (r Values) for Various Species[a]

	Ozone	H_2O	CO	Methane	Ethane	Ethyne	Propane	n-Butane	i-Butane	PAN	Aerosol σ_{ap}	Aerosol σ_{sg}	Aerosol σ_{bsg}	C_2Cl_4
Ozone	(1.00)													
H_2O	-0.60	(1.00)												
CO	0 36	-0.23	(1.00)											
Methane	0.34	-0.22	0.77	(1.00)										
Ethane	0 42	-0.37	(0.87)	(0 82)	(1.00)									
Ethyne	0.41	-0 38	(0.90)	0 76	(0.92)	(1.00)								
Propane	0.35	-0.42	0 75	0.78	(0 92)	(0.90)	(1.00)							
n-Butane	0.26	-0.34	0.62	0 66	(0.81)	(0 83)	(0 96)	(1.00)						
i-Butane	0.27	-0.39	0 64	0.68	(0 80)	(0.84)	(0.94)	(0.93)	(1.00)					
PAN	0.37	-0.53	0.66	0.40	0.59	0.72	0.62	0 59	0.65	(1.00)				
Aerosol σ_{ap}	0.31	-0.38	0.31	0.05	0.15	0 27	0.07	0 06	0 04	0.69	(1.00)			
Aerosol σ_{sg}	0.34	-0.36	0.40	0.11	0.26	0 34	0 16	0.13	0.12	0.65	(0.95)	(1.00)		
Aerosol σ_{bsg}	0.44	-0 49	0.31	0 04	0.17	0.25	0 06	0.03	0.03	0.70	(0.94)	(0.94)	(1.00)	
C_2CL_4	0.37	-0.17	0.70	0.54	0 64	0.71	0.64	0.61	0.65	0.54	0.09	0.09	0.06	(1.00)

[a]The r values in parentheses are those whose absolute value is greater than or equal to 0.80. The linear correlations were determined from leg averages, but excluding instances where the data was contaminated by local pollution or stratospheric sources (see text).

STP) through the inlet. The NO instrument sampled air prior to the metal bellows pump at ambient pressure. The metal bellows pump supplied air to the Dasibi, and a cabin vent in front of the Dasibi insured that the instrument was at cabin pressure.

The Dasibi was calibrated in the laboratory against a CSI Photocal 3000 ozone generator prior to installation on the plane; and calibrated again on board the aircraft through the sampling inlet. The two calibration slopes differed by 4%, indicating a 4% loss of ozone when sampled through the aircraft inlet and bellows pump. The detection limit of the Dasibi during these flights was about 2 ppbv; the overall uncertainty of the data was of the order of 1 ppbv.

A2. NO

The NO instrument was constructed and tested in our research laboratories at the University of Alaska-Fairbanks and the University of Washington-Seattle. The measurement of NO used the principle of chemiluminescence; ambient NO was reacted with excess ozone in a low-pressure dynamic flow reaction chamber, and photons from decay of the product, $NO_2^*(^2B_1)$, were detected by a photomultiplier tube [*Kley and McFarland*, 1980; *Drummond et al.*, 1985; *Ridley and Grahek*, 1990].

NO was quantitatively measured by switching between four modes of operation: measure, zero, calibration, and calibration zero. A 20 min measurement cycle was used during the experiment to coincide with the flight legs. It consisted of 9 min for measurements, 6 min for zeroing, and 5 min for calibration.

Air at ambient pressure was sampled from the 3/8 inch ID Teflon sample line (as described above) and entered the NO instrument through a 1/4 inch ID Teflon tube. The sample then passed through a 47 mm Teflon filter holder containing a 1.0 μm Teflon filter. The air sample was mass flow controlled at 1 standard leter per minute (sLmp). Upstream of the mass flow controller the airstream was at ambient pressure, and downstream it was 82 torr. The sample then passed over a water vapor addition system. This system was made from a 47 mm Teflon filter holder that was used as a 30 mL water reservoir and heated to 70°C. The filter holder contained a 1.0 μm Teflon filter that allowed water vapor to pass but isolated liquid water from the sample stream. Water vapor addition was approximately 1 g h^{-1}. The humidified sample stream then entered a zeroing volume consisting of a 4 foot segment of 3/8 inch ID Teflon tubing with a total volume of 86.9 mL. Subsequent to the zeroing volume, the sample stream entered the reaction chamber and mixed with ~4% O_3 in O_2 from the ozone generator. The reaction chamber was based on the design of *Ridley and Grahek* [1990], only differing slightly from their design in its mounting to the PMT cooler. The Ridley and Grahek design was simplified by eliminating one flange, resulting in a closer fit and one less window. The reaction chamber was temperature-controlled at 30°C. During operation the measured reaction chamber pressure was between 5 and 6 torr, which compared reasonably well with expectations (4 torr) given the 200 Lpm pumping speed of the vacuum pump and some loss of efficiency due to tubing connections. The sample stream exited the reaction chamber through a 1 inch ID stainless steel bellows tube connected to a two-stage vacuum pump equipped with a reactive gas trap filled with Hopcalite catalyst for ozone removal. The pump used Fomblin perfluorinated pump oil.

A red RG 610 Schott filter was placed between the PMT and the reaction chamber, blocking wavelengths shorter than 610 nm. The PMT was a dry ice cooled, red-sensitive, Hamamatsu R-1333. The signal from the PMT was amplified by a photomultiplier amplifier discriminator, converted to a transistor-transistor logic (TTL) signal, and read by a PCM-DAS16D/16 data acquisition card installed on a laptop computer. The computer read the count rate every 0.1 s, accumulated 10 readings, and output the signal as counts per second.

The ozone generator used a high-voltage discharge corona to generate roughly 4% O_3 in O_2. The pressure inside the ozone generator was kept at approximately 1 atm, and it received a flow of 0.200 sLpm O_2 maintained by a mass flow controller. The bulk of the O_3 in O_2 mixture entered the NO instrument and was directed into the reaction chamber.

The signal was zeroed in "zero" and "calibration zero" modes by diverting roughly 5% of the flow from the ozone generator into the sample stream just prior to the zeroing volume, with the remaining 95% of the ozone flow continuing to the reaction chamber. Zeroing efficiencies between 95 and 99% were achieved.

Calibrations were performed with a NO calibration standard from Scott-Marrin Inc (1.001 ppmv ± 2%, NO in N_2). During calibrations a mass flow controller delivered 4 cm^3 min^{-1} STP of NO in N_2 to the sample stream.

For safety considerations the NO instrument could not run continuously between flights on board the King Air. Installing and removing the instrument from the plane before and after each flight was also not practical. Hence it was necessary to restart the instrument before each flight. A warm-up time of 3 hours was sufficient for zero mode signal stabilization. However, the sensitivity of the instrument to NO took much longer to stabilize. Generally the sensitivity did not stabilize for the duration of a flight. Hence we measured the sensitivity frequently, once during each flight leg, and the sensitivity at any given time was determined by linear interpolation between each calibration. The sensitivity generally increased throughout a flight and ranged between 3.5 and 4.5 counts per second (cps) per pptv NO for a 5 hour flight. On the basis of laboratory tests the sensitivity stabilized after 12-24 hours of operation.

Following the 3 hour warm-up, the zero level was stable, except it tended to increase as a function of altitude due to the increasing effects of cosmic rays on the PMT. The increase was typically 10% from sea level to 8 km.

The NO instrument signal was quality-controlled to remove anomalous spikes in the data caused by interference from the aircraft's communications system and corrected for instrument switching response time constants, ambient humidity fluctuations, and NO loss in the sample lines due to reaction with ambient ozone. The instrument's zero signal and sensitivity showed no dependence to variations in ambient pressure. However, ambient humidity changes, while mitigated by the use of a water vapor addition system, still had a small effect. The effects of ambient humidity fluctuation on zero signal and sensitivity were characterized in our laboratory at the University of Washington. Corrections to the NO data due to humidity fluctuations were small, generally less than 1%. Signal spikes caused by the communications system accounted for less than 1% of the overall data; the other corrections were of the order of 5% or less in total. Extensive leak testing of the instrument and sample lines revealed no detectable cabin air leaks into the instrument.

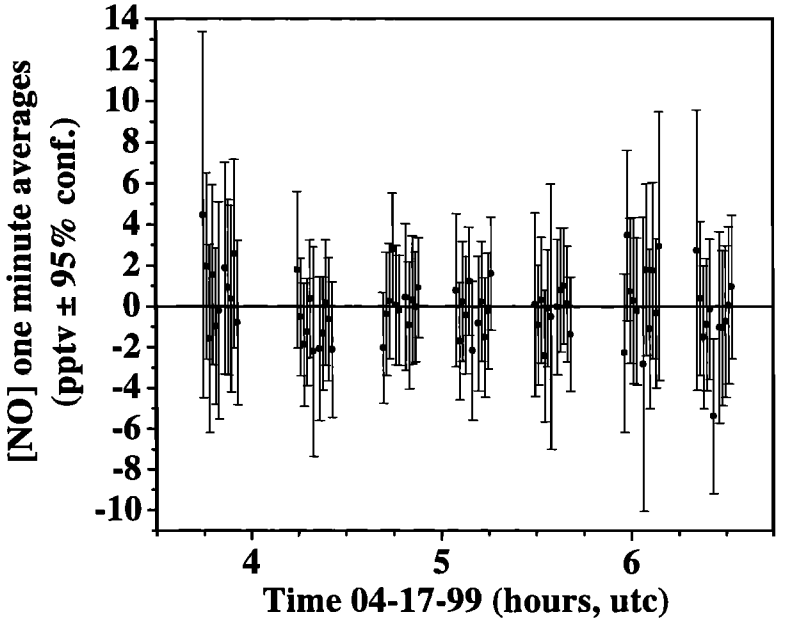

Figure 7. Mixing ratio (pptv) of NO during the PHOBEA night flight on April 17, 1999. Because of the reaction of O_3 with NO, we expect a value of zero.

Determining the presence of signal artifacts is critical for the measurement of NO when its concentration is low [*Drummond et al.*, 1985]. Signal artifacts are an instrument zero offset, most easily detected as nonzero measurements in the absence of analyte. Artifacts can be caused by, among other things, interfering compounds which chemiluminesce, significant fluctuations in ozone concentration from the ozone generator, and cabin air leaks into the sampling lines.

There are two standard methods to monitor instrumental artifacts. Because NO is quickly converted to NO_2 by ambient ozone in the absence of light, the most reliable method is to measure NO at night in a region remote from sources of NO. Any significant deviation from 0 pptv likely reflects instrumental artifacts. A less reliable method is to measure the NO concentration in cylinders of high-quality synthetic zero air. Zero air cylinders, however, may contain mixing ratios of up to a few pptv NO, thus making these tests somewhat less conclusive.

Artifact tests were made during one night flight and with zero air measurements before each flight. The mean NO mixing ratio measured on the night flight was -0.1 ± 1.6 pptv (mean plus or minus one standard deviation, N = 63 one-min averages). Figure 7 depicts NO measurements during the night flight. Zero air measurements had more variability than the night flight measurements, but also centered around 0 pptv NO. From 16 measurements made throughout the aircraft campaign, the mean NO mixing ratio in zero air was -0.3 ± 2.9. On the basis of these tests the NO instrument was considered free of significant artifacts during this experiment.

The 2σ detection limit of this instrument was on average 2 pptv NO for a 9 min signal integration time and 4 pptv for a 1 min signal integration time. The instrument precision was on average ±4 pptv at the 95% confidence interval for a 1 min signal integration time.

A3. PAN

The PAN instrument was a significantly modified gas chromatographic system supplied by Meteorologie Consult GmbH, Glashütten, Germany (MetCon). Chromatography was based on a dual megabore capillary column system (precolumn: DB-1, 5 m, and analytical column: DB-5, 7 m) maintained at a constant temperature of 20°C by a Peltier cooler, and a Fisons 800 electron capture detector (ECD) maintained at 30°C. An MKS Baratron (model 640A) constant pressure transducer maintained the pressure in the ECD at 900 torr at all times. The carrier gas was ultrahigh purity (UHP) N_2 (Scott Marrin) maintained at 20 mL min^{-1} through each column by an MKS (model 1179A) mass flow controller. One mass flow controller was used, and when the flows through both columns were separate (see below), they were kept approximately the same by the use of additional flow restrictors.

Air was brought into the system through a 1/4 inch ID Teflon-lined backward facing inlet. Approximately 4 m of Teflon tubing connected the instrument to the inlet, with a 47 mm diameter 0.5 μm Teflon filter at the instrument end. The sample flow through the inlet was kept at 500 mL min^{-1}, and of this inlet flow 50 mL min^{-1} was fed to a 1 mL sample loop which consisted of uncoated quartz capillary tubing (0.53 mm bore). An MKS Baratron (model 722A) pressure transducer continually monitored the pressure of the sampled air in the sample loop. Because flow control was based on capillary flow restrictors, which resulted in flow variations with ambient pressure, both the main and secondary flow were monitored with Brooks Mass Rate (model 5700) mass flowmeters to ensure that sufficient flow was fed to the sample loop.

An ambient sample was injected every 5 min onto the precolumn by switching a 10 port valve (Valco, model W). By using a second 4 port valve (Valco, model W), the first 45 s of

the precolumn eluent were sent to a bypass channel to elute the (oxygen) solvent peak which tends to overload the detector. At the same time, pressure fluctuations due to sample injection were abated. Forty-five seconds into a run the 4 port valve was switched, and the precolumn and analytical column were then in series. After 2.2 min into the run, the 10 port valve was switched back to load a subsequent ambient sample in the sample loop, while at the same time the precolumn was backflushed to remove higher boiling compounds.

A Campbell Scientific Inc. (CSI) 21X data logger controlled the instrument and acquired the data. All instrument signals were stored in a CSI storage module for download to laptop computer at the completion of each flight.

In-flight span/calibration of the gas chromatographic (GC) system was made every 20 min, during each sampling leg, using a commercial PAN calibrator (MetCon). Multipoint calibrations were also performed on the ground using the same instrument. The calibrator generated PAN from the photolysis of acetone mixed with NO in air. A constant flow of 30 mL min^{-1} ultrazero (UZ) air (Scott Marrin, monitored by a Brooks Mass Rate model 5700 mass flowmeter) was passed through a small permeation vessel filled with reagent grade acetone and then mixed with a flow of 1 mL min^{-1} NO in N_2 (Scott Marrin, certified at 1.001 ppmv ± 2% NO, maintained by a MKS model 1179A mass flow controller). Photolysis of the acetone was done with a Hg Pen-Ray lamp with wavelengths below 300 nm filtered out. The conversion of NO into PAN has been shown to be 90 ±5 % complete [*Volz-Thomas et al.*, 1996]. The resultant flow of PAN was diluted with variable amounts of zero air (controlled by a MKS model 1179A mass flow controller) yielding PAN mixing ratios of 150-1000 pptv. During the PHOBEA experiments the in-flight span was set at 500 pptv.

The detection limit was linearly dependent on ambient pressure and was determined from laboratory measurements to be 15 pptv at 760 torr and 45 pptv at 400 torr. PAN measurements below the detection limit of the instrument were set to one half the detection limit for statistical calculations.

The PAN instrument precision and accuracy were also pressure-dependent. At 760 torr the precision was better than 50% at 20 pptv and better than 10% at 40 pptv. However, because of a pressure correction factor, precision was worse at higher altitudes. For example, this correction factor was 3 at 6.5 km, resulting in a precision which was better than 50% at 60 pptv at that altitude. Taking all uncertainties into consideration (including flow controller calibrations, standards, efficiency of PAN production in the calibrator unit), the accuracy was estimated at 30% below 100 pptv at 760 torr, with a similar scaling as the precision at lower pressures.

A4. CO, CH_4, and VOCs

A total of 46 pressurized whole air samples were collected in stainless steel canisters for GC-flame ionization detection and electron capture detection analysis of CO, CH_4, and VOCs [*Blake et al.*, 1994]. Air samples were drawn from a 1 cm ID rearward facing stainless steel inlet, then through 2 m of stainless steel tubing and a stainless steel metal bellows pump at a pumping speed of roughly 15 Lpm (at sea level). The sample lines on the high-pressure side of the bellows pump were pressurized and purged several times before filling the canisters to between $1.38x10^5$-$2.76x10^5$ Pa. An average of three samples were taken per flight.

Two of the forty-six whole air samples contained anomalously high VOC levels, several orders of magnitude higher than all other samples. These two samples were inconsistent with other measurements made at the same time (e.g., NO and aerosols), which indicated a relatively clean air mass. We assumed these two canisters became contaminated during handling and were excluded during our analysis.

A5. Aerosol Measurements

Sample air was drawn at 30 Lpm through a 1 cm ID rearward facing stainless steel inlet in order to exclude cloud droplets and through 3 m of 1 cm ID conductive tubing to the aerosol instruments. Total light scattering at 450, 550, and 700 nm (referred to as $\sigma_{sp}(450)$, $\sigma_{sp}(550)$, and $\sigma_{sp}(700)$ below, respectively) and hemispheric backscattering at the same three wavelengths ($\sigma_{bsp}(450)$, $\sigma_{bsp}(550)$, and $\sigma_{bsp}(700)$, respectively) were measured with an integrating nephelometer (TSI model 3563). No size restriction was used on the nephelometer, but with a rearward facing inlet, only small aerosols would be sampled. This device was calibrated with gases of known scattering and backscattering coefficients (air and CO_2). Measurements of the calibration gases were made twice during the campaign, and zerooffsets were determined by sampling filtered air during both outbound and inbound ferry portions of each flight. Corrections were applied as recommended by *Anderson and Ogren* [1998].

Light absorption at 550 nm ($\sigma_{ap}(550)$) was measured with a differential transmission absorption photometer (Radiance Research, model PSAP). This device was calibrated by the manufacturer, and calibration corrections, including a correction for response to light scattering, were made as recommended by *Bond et al.* [1999].

The number density of particles larger than 10 nm diameter was measured with a condensation particle counter (CPC; TSI, Inc., model 3010). The PSAP and CPC measurements were made immediately downstream of the nephelometer. Upstream of the nephelometer was a ball valve and high efficiency particulate air (HEPA) filter arrangement that allowed manual switching to filtered, particle-free air. All aerosol concentrations have been corrected to STP.

A6. $J(NO_2)$

The NO_2 photodissociation frequency was measured utilizing two $J(NO_2)$ radiometers (MetCon). Each radiometer provided a nearly isotropic response over a solid angle of 2π steradians and used a Schott 2xUG3, UG5 filter combination. The theory behind these measurements is described by *Junkermann et al.* [1989]; *Volz-Thomas et al.* [1996] estimated the uncertainty of a similar instrument to be 8% under clear-sky conditions.

$J(NO_2)$ data measured with radiometers are subject to three corrections; for spectral response, angular response, and temperature. The spectral correction is small, but depends on altitude and solar zenith angle. Discrete correction values from the manufacturer were fitted to a polynomial expression allowing for correction at all altitudes and zenith angles ≤80°. This correction was of the order of 0-5%. An angular correction is necessary at zenith angles larger than 80° [*Volz-Tho-*

mas et al., 1996], but because all of our daytime flights were centered on solar noon, no angular corrections were necessary. The manufacturer calibrated our transfer standard at 25°C; however, the sensitivity increased slightly with decreasing temperatures. We used the temperature correction described by *Volz-Thomas et al.* [1996].

The radiometers were mounted on the top and bottom of the aircraft fuselage and were not pressurized. The two sensors were calibrated against a similar instrument from Met-Con, which we used as a transfer standard. The calibration was performed after the aircraft campaign on top of the roof of the Department of Atmospheric Sciences building at the University of Washington. The transfer standard radiometer has been used by the Jaffe research group since 1995 and has been calibrated yearly against a set of master $J(NO_2)$ radiometers, which were calibrated by the Forschungszentrum Jülich, Germany, against a chemical actinometer.

We also checked the accuracy of our $J(NO_2)$ measurements by comparing the aircraft data with $J(NO_2)$ calculated from a radiative transfer model. We compared 109 min of cloud-free $J(NO_2)$ measurements between 0-2 km with calculations of $J(NO_2)$ using a four-stream radiative transfer model (S. Madronich, National Center for Atmospheric Research (NCAR), personal communication, 2000). The model [*Madronich and Flocke*, 1998] used a pseudospherical four-stream discrete ordinates radiation scheme (NO_2 cross sections and quantum yields from *DeMore et al.* [1997]). The model was set to calculate downwelling $J(NO_2)$ at Cheeka Peak Observatory (i.e., at 0.5 km, 48.30°N, 124.62°W), with a surface albedo of 0.1, and during cloud-free conditions. The resulting $J(NO_2)$ from the model, corresponding to the dates and times of our cloud-free aircraft measurements, was 7.77×10^{-3} s^{-1}. Our cloud-free aircraft measurements of downwelling $J(NO_2)$ were $7.86 \times 10^{-3} \pm 0.71 \times 10^{-3}$, 0.50×10^{-3} s^{-1} (mean plus or minus one standard deviation, 95% confidence interval) at an average location of 1.1 km, 47.91°N, and 126.95°W. Hence our $J(NO_2)$ measurement accuracy compares well with model calculations, and the instrumental uncertainty compares well with that reported by *Volz-Thomas et al.* [1996].

A7. NO_2 and NO_x

NO_2 was computed from a simple model using the photostationary state approximation (Leighton relationship)

$$[NO_2] = \frac{[NO]\,[O_3]\,k_{NO-O_3}}{J(NO_2)} \qquad (7)$$

where $k_{NO\text{-}O3}$ is the NO + O_3 reaction rate constant ($k_{NO\text{-}O3} = 2 \times 10^{-12} \times e^{(-1400/T)}$ *DeMore et al.* [1997]) and T (K) is the ambient temperature. However, equation (7) tends to underestimate the NO_2 mixing ratio because it neglects the contribution of peroxy radicals in the conversion of NO to NO_2 [*Hauglustaine et al.*, 1999]. Hence NO_2 calculated from equation (7) should be considered a lower limit to the actual mixing ratio. Hauglustaine et al. found that (7) underestimated the NO_2 mixing ratio by a factor of 2 during springtime measurements on Mauna Loa, Hawaii.

NO_x was computed as the sum of measured NO and model-calculated NO_2.

A8. Aircraft Data

A listing of the standard instrumentation on board the King Air, its precision, and accuracy can be found on the web site of the University of Wyoming's Department of Atmospheric Science (http://www-das.uwyo.edu/). Data sampling, recording, and processing were controlled by an onboard data acquisition system and displayed with a Sun workstation.

Water vapor mixing ratios were calculated from dew and frost point measurements made with a chilled mirror instrument (Cambridge, model 137C3). The measurements were reliable above –50°C and accurate to ±1°C above 0°C and ±2°C below 0°C.

Acknowledgments. We would like to thank Bill Simpson at the University of Alaska-Fairbanks for his role in building the NO instrument and his advice in its testing and development, Sasha Madronich at NCAR for his model calculations of $J(NO_2)$, and the University of Wyoming flight crew and pilot, whose efforts were indispensable in the success of this project. This work was supported by the National Science Foundation grant ATM989627.

References

Akimoto, H., and H. Narita, Distribution of SO_2, NO_x, and CO_2 emissions from fuel combustion and industrial activities in Asia with 1°x1° resolution, *Atmos. Environ.*, *28*, 213-225, 1994.

Anderson, T. L., and J. A. Ogren, Determining aerosol radiative properties using the TSI 3563 integrating nephelometer, *Aerosol Sci. Technol.*, *29*, 57-69, 1998.

Andreae, M. O., H. Berresheim, T. W. Andreae, M. A. Kritz, T. S. Bates, and J. T. Merrill, Vertical distribution of dimethylsulfide, sulfur dioxide, aerosol ions, and radon over the northeast Pacific Ocean, *J. Atmos. Chem.*, *6*, 149-173, 1988.

Bailey, R., L. A. Barrie, C. J. Halsall, P. Fellin, and D. C. G. Muir, Atmospheric organochlorine pesticides in the western Canadian Arctic: Evidence of transpacific transport, *J. Geophys. Res.*, *105*, 11,805-11,811, 2000.

Berntsen, T., S. Karlsdottir, and D. Jaffe, Influence of Asian emissions on the composition of air reaching the northwestern United States, *Geophys. Res. Lett.*, *26*, 2171-2174, 1999.

Blais, J. M., D. W. Schindler, D. C. G. Muir, L. E. Kimpe, D. B. Donald, and B. Rosenberg, Accumulation of persistent organochlorine compounds in mountains of western Canada, *Nature*, *395*, 585-588, 1998.

Blake, D. R., T. W. Smith Jr., T. -Y. Chen, W. J. Whipple, and F. S. Rowland, Effects of biomass burning on summertime nonmethane hydrocarbon concentrations in the Canadian wetlands, *J. Geophys. Res.*, *99*, 1699-1719, 1994.

Blake, N. J., D. R. Blake, T. Chen, J. E. Collins, G. W. Sachse, B. E. Anderson, and F. S. Rowland, Distribution and seasonality of selected hydrocarbons and halocarbons over the western Pacific basin during PEM-West A and PEM-West B, *J. Geophys. Res.*, *102*, 28,315-28,331, 1997.

Bond, T. C., T. L. Anderson, and D. Campbell, Calibration and intercomparison of filter-based measurements of visible light absorption by aerosols, *Aerosol Sci. Technol.*, *30*, 582-600, 1999.

Brasseur, G. P., J. J. Orlando, and G. S. Tyndall, *Atmospheric Chemistry and Global Change*, Oxford Univ. Press, New York, 1999.

Cooper, O. R., J. L. Moody, J. C. Davenport, S. J. Oltmans, B. J. Johnson, X. Chen, P. B. Shepson, and J. T. Merrill, Influence of springtime weather systems on vertical ozone distributions over three North American sites, *J. Geophys. Res.*, *103*, 22,001-22,013, 1998.

Corbett, J. J., P. S. Fischbeck, and S. N. Pandis, Global nitrogen and sulfur inventories for oceangoing ships, *J. Geophys. Res.*, *104*, 3457-3470, 1999.

DeMore, W. B., S. P. Sander, C. J. Howard, A. R. Ravishankara, D. M. Golden, C. E. Kolb, R. F. Hampson, M. J. Kurylo, and M. J.

Molina, Chemical kinetics and photochemical data for use in stratospheric modeling, *JPL Publ., 97-4*, 1997.

Drummond, J. W., A. Volz, and D. H. Ehhalt, An optimized chemiluminescence detector for tropospheric NO measurements, *J. Atmos. Chem.*, *2*, 287-306, 1985.

Elbern, H., J. Hendricks, and A. Ebel, A climatology of tropopause folds by global analyses, *Theoretical Appl. Climatol.*, *59*, 181-200, 1998.

Elliott, S., D. R. Blake, R. A. Duce, C. A. Lai, I. McCreary, L. A. McNair, F. S. Rowland, A. G. Russell, G. E. Streit, and R. P. Turco, Motorization of China implies changes in Pacific air chemistry and primary production, *Geophys. Res. Lett.*, *24*, 2671-2674, 1997.

Greenberg, J. P., D. Helmig, and P. R. Zimmerman, Seasonal measurements of nonmethane hydrocarbons and carbon monoxide at the Mauna Loa Observatory during the Mauna Loa Observatory Photochemistry Experiment 2, *J. Geophys. Res., 101*, 14,581-14,598, 1996.

Gregory, G. L., J. T. Merrill, M. C. Shipman, D. R. Blake, G. W. Sachse, and H. B. Singh, Chemical characteristics of tropospheric air over the Pacific Ocean as measured during PEM-West B: Relationship to Asian outflow and trajectory, *J. Geophys. Res., 102*, 28,275-28,285, 1997.

Guderian, R., D. T. Tingey, and R. Rabe, Effects of photochemical oxidants on plants, in *Air Pollution by Photochemical Oxidants: Formation, Transport, Control, and Effects on Plants*, edited by R. Guderian, pp. 127-333, Springer-Verlag, New York, 1985.

Hauglustaine, D., S. Madronich, B. Ridley, S. J. Flocke, C. A. Cantrell, F. L. Eisele, R. E. Shetter, D. L. Tanner, P. Cinoux, and E. L. Atlas, Photochemistry and budget of ozone during the Mouna Loa Observatory Photochemistry Experiment (MLOPEX2), *J. Geophys. Res., 104*, 30,275-30,307, 1999.

Hoell, J. M., D. D. Davis, S. C. Liu, R. Newell, M. Shipham, H. Akimoto, R. J. McNeal, R. J. Bendura, and J. W. Drewry, Pacific Exploratory Mission-West A (PEM-West A): September-October 1991, *J. Geophys. Res., 101*, 1641-1653, 1996.

Hoell, J. M., D. D. Davis, S. C. Liu, R. E. Newell, H. Akimoto, R. J. McNeal, and R J. Bendura, Pacific Exploratory Mission-West Phase B: February-March 1994, *J. Geophys. Res., 102*, 28,223-28,239, 1997.

Horowitz, L. W., and D. J. Jacob, Global impacts of fossil fuel combustion on atmospheric NO_x, *J. Geophys. Res., 104*, 23,823-23,840, 1999.

Hübler, G., D. W. Fahey, B. A. Ridley, G. L. Gregory, and F. C. Fehsenfeld, Airborne measurements of total reactive odd nitrogen (NO_y), *J. Geophys. Res., 97*, 9833-9850, 1992.

Jacob, D. J., J. A. Logan, and P. P. Murti, Effect of rising Asian emissions on surface ozone in the United States, *Geophys. Res. Lett., 26*, 2175-2178, 1999.

Jaffe, D., et al., Transport of Asian air pollution to North America, *Geophys. Res. Lett., 26*, 711-714, 1999.

Jaffe, D., T. Anderson, D. Covert, B. Trost, J. Danielson, W. Simpson, D. Blake, and J. Harris, Observations of ozone and related species in the northeast Pacific during the PHOBEA campaigns, 1, Ground-based observations at Cheeka Peak, *J. Geophys. Res.*, this issue.

Junkermann, W., U. Platt, and A. Volz-Thomas, A photoelectric detector for the measurement of photolysis frequencies of ozone and other atmospheric molecules, *J. Atmos. Chem., 8*, 203-227, 1989.

Kley, D., and M. McFarland, Chemiluminescence detector for NO and NO_2, *Atmos. Technol., 12*, 63-69, 1980.

Kondo, Y., M. Koike, S. Kawakami, H. B. Singh, H. Nakajima, G. L. Gregory, D. R. Blake, G. W. Sachse, J. T. Merrill, and R. E. Newell, Profiles and partitioning of reactive nitrogen over the Pacific Ocean in winter and early spring, *J. Geophys. Res., 102*, 28,405-28,424, 1997.

Madronich, S. and S. Flocke, The role of solar radiation in atmospheric chemistry, in *Handbook of Environmental Chemistry*, edited by P. Boule, pp. 1-26, Springer-Verlag, New York, 1998.

Moxim, W., H. Levy, and P. Kasibhatla, Simulated global tropospheric PAN: Its transport and impact on NO_x, *J. Geophys. Res., 101*, 12,621-12,638, 1996.

Parrish, D. D., C. J. Hahn, E. J. Williams, R. B. Norton, F. C. Fehsenfeld, H. B. Singh, J. D. Shetter, B. W. Gandrud, and B. A. Ridley, Indications of photochemical histories of Pacific air masses from measurements of atmospheric trace species at Point Arena, California, *J. Geophys. Res., 97*, 15,883-15,901, 1992.

Ridley, B. A., and F. E. Grahek, A small, low flow, high sensitivity reaction vessel for NO chemiluminescence detectors, *J. Atmos. Oceanic Technol., 7*, 307-311, 1990.

Ridley, B. A., M. A. Carroll, D. D. Dunlap, M. Trainer, G. W. Sachse, G. L. Gregory, and E. P. Condon, Measurements of NO_x over the eastern Pacific Ocean and southwestern United States during the spring 1984 NASA GTE aircraft program, *J. Geophys. Res., 94*, 5043-5067, 1989.

Ridley, B. A , E. L. Atlas, J. G. Walega, G. L. Kok, T. A. Staffelback, J. P. Greenberg, F. E. Grahek, P. G. Hess, and D. D. Montzka, Aircraft measurements made during the spring maximum of ozone over Hawaii: Peroxides, CO, O_3, NO_y, condensation nuclei, selected hydrocarbons, halocarbons, and alkyl nitrates between 0.5 and 9 km altitude, *J. Geophys. Res., 102*, 18,935-18,961, 1997.

Streets, D. G., and S. T. Waldhoff, Present and future emissions of air pollutants in China: SO_2, NO_x, and CO, *Atmos. Environ., 34*, 363-374, 2000.

Talbot, R. W., et al., Chemical characteristics of continental outflow from Asia to the troposphere over the western Pacific Ocean during February-March 1994: Results from PEM-West B, *J. Geophys. Res., 102*, 28,255-28,274, 1997.

VanAardeen, J., G. Carmichael, H. Levy, D. Streets, and L. Hordijk, Anthropogenic NO_x emissions in Asia in the period 1990-2020, *Atmos. Environ., 33*, 633-646, 1999.

Volz-Thomas, A., A. Lerner, H.-W Patz, M. Schultz, D. S. McKenna, R. Schmitt, S. Madronich, and E. P. Röth, Airborne measurements of the photolysis frequency of NO_2, *J. Geophys. Res., 101*, 18,613-18,627, 1996.

T. L. Anderson, Department of Atmospheric Sciences, University of Washington, Seattle, WA 98195.

H. J. Beine, CNR-Istituto sull'Inquinamento Atmosferico, Via Salaria Km 29.300, CP10, I - 00016 Monterotondo Stazione, Roma, Italy.

D. R. Blake, Department of Chemistry, University of California, Irvine, CA 92717.

J. W. Bottenheim, Atmospheric Environment Service, Toronto, Ontario M3H 5T4, Canada.

J. M. Harris, Climate Monitoring and Diagnostics Laboratory, NOAA, Boulder, CO 80303.

D. A. Jaffe, Interdisciplinary Arts and Sciences, University of Washington, Bothell, WA 98021. (djaffe@u.washington.edu)

R. A. Kotchenruther, Department of Chemistry, University of Washington, Seattle, WA 98195.

R. Schmitt, Meteorologie Consult GmbH, Auf der Platt 47, D-61479 Glashütten, Germany.

(Received April 25, 2000; revised July 11, 2000;
accepted July 19, 2000.)